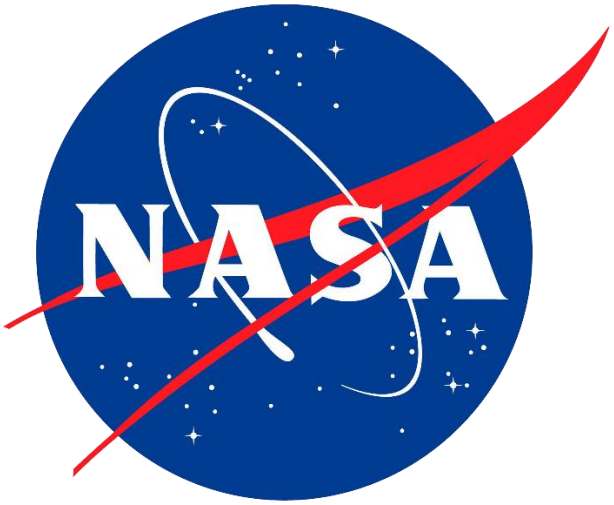
NDSU MECHANICAL ENGINEERING

NASA X-Hab Power Rover 2.0

Nick Becker, Remy Darr, Nick Fahnlander, Evan Paulson

PI: Dr. Jessica Vold

Co-PIs: Dr. Bora Suzen and Dr. Ali Amiri



Department of Mechanical Engineering
North Dakota State University
Fall 2025 – Spring 2026

Table of Contents

1. Executive Summary 2
2. Design Problem and Objectives 2
3. Detailed Design Documentation 3

Conceptual Design 3

ROVER SELECTION 3
STATION SELECTION 11

Detailed Design Documentation 15

MOTOR SELECTION 15
SOLAR PROTECTION 16
Roller Motor *17*
Bevel Gear *17*
Spring *18*
MAIN CONTROLLERS 18
SERVOS 19
FRAME 19
SUSPENSION ASSEMBLY 21
WHEEL ASSEMBLY 24
STATION 26
CHARGING CONNECTION 29
FINAL SYSTEM DESIGN 30
REDESIGNS 31
MANUFACTURING 38
Rover Body *38*
Suspension and Drive Train *42*
Electrical *46*
STATION 48
Charging Connection *51*

4. Laboratory Test Results 51
5. Conclusions 54
6. Future Work and Recommendations 54

CAMBERING 54
SERVOS AND HUB MOTORS 55
CHARGER ALIGNMENT 55
SOLAR FILM 55

7. References 56

1. Executive Summary

This project focuses on developing a rover and station system designed to charge and revive other rovers that have entered a critically low-power state. The primary objective is to ensure mission continuity and rover recovery in remote or power-limited environments where solar energy is unavailable or insufficient. By enabling mobile energy delivery, the system increases the operational lifespan of field-deployed rovers and prevents the permanent loss of valuable equipment.

The rescue rover is engineered to travel long distances, navigate challenging terrain, and deliver power directly to disabled rovers. Its charging capabilities are designed to be efficient, reliable, and flexible enough to support a variety of rover platforms. Complementing this is an immobile charging station that is able to recharge the rescue rover and provide additional charging for future expansion as more rovers are deployed. This station will also serve as the charging interface proof of concept.

The design process includes system requirements definition, mobility and energy-transfer analysis, navigation considerations, prototype development, and validation of successful charging operations. The completed system demonstrates a scalable and self-sustaining approach to maintaining rover networks, particularly in remote research sites, planetary environments, or hazardous areas where human intervention is not feasible.

2. Design Problem and Objectives

Rovers operating on planetary surfaces often become permanently disabled when they enter a critical low-power state and are unable to recharge. Once a rover can no longer generate or store sufficient energy, such as during extended darkness, dust accumulation, or loss of solar input, its mission ends prematurely. This failure not only shortens the rover's operational lifespan but also results in the loss of significant scientific investment.

The objective of this project is to develop a system capable of demonstrating charging and reviving these low-power rovers so they can resume their missions instead of becoming irrecoverable. To address this problem, a self-powered rescue rover was proposed, equipped to deliver energy to a wide range of rover platforms. It must be capable of traveling to remote locations where solar energy is unavailable along with when environmental conditions are harsh, and terrain is difficult to navigate.

This rover will operate alongside a charging station designed to maintain the rover's own energy levels while supporting future fleet expansion. The combined system ensures sustainable operation and the ability to perform repeated rescue missions.

Cost implications primarily arise from the need for highly reliable components that can withstand extreme temperatures, abrasive regolith, and rugged terrain while remaining durable over long mission intervals. Materials must be selected to prevent dust-related wear, support mobility in cold environments, and ensure the charging system remains dependable under varying loads.

The design of the rescue rover is governed by a series of strict environmental, operational, and budgetary constraints. The system must operate reliably across extreme planetary temperature ranges from −173 °C to 127 °C. Terrain conditions, including large rocks, steep inclines, and highly uneven surfaces, require a robust mobility system capable of maintaining traction and stability. In addition, all mechanical and electrical components must resist degradation from fine regolith particles, ensuring that dust does not cause significant wear or interfere with moving parts. The rover must deliver at least 50 W of charging power to revive other rovers and support mission sustainability while remaining cost-effective by incorporating only essential features within the project's budget limits. Size and mass are also constrained, with a target weight of under 500lbs and an allowable footprint smaller than that of the Curiosity rover at approximately 9 feet in length and 7 feet in width [1]. Furthermore, the rover must store 2000Wh of usable onboard energy, endure mechanical loads of 2G during operation or transport, and maintain a steady travel speed of about 0.667 mph to reach disabled rovers efficiently. These constraints are compounded by the requirement that critical components and materials must be obtainable within a tow to three month lead time, ensuring the feasibility of the build schedule. NASA also requires a 1.4 Factor of Safety as defined in the NASA Technical Standard for Structural Design and Test Factors of Safety for Spaceflight Hardware [2,3].

3. Detailed Design Documentation

Conceptual Design

Rover Selection

Ten concepts were generated for a rover that can collect energy and charge with a station. Each team member was tasked with generating two concepts, the power rover 1.0 was the ninth, and as a team the tenth concept was generated. These concepts were put into a screening matrix and assigned a relative score to the baseline concept 3, then after selecting and combining, four designs were chosen to advance to the scoring process.

Concept 1 seen in Figure 1 is a four wheeled rover with a central drive motor and chain drives. Steering is tank style with the wheels on each side being locked in rotation with each other. It has a solar panel on a robotic arm that can track the sun for power. Additionally, it has a detachable Radioisotope Thermoelectric Generator (RTG) that provides power and can be removed when the rover has to travel across more difficult terrain.

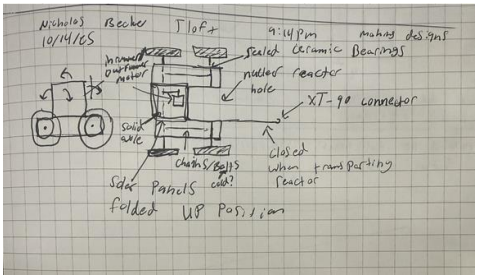


Figure 1: Rover Concept 1

Concept 2 seen in Figure 2 is a four wheeled rover with hub motors that are independently steered by stepper motors. It is powered by foldable solar panels that can track the sun with one axis of tilt. It includes a trailer hitch to connect to a trailer-like station.

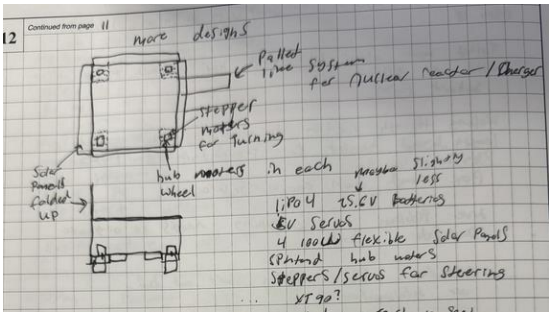


Figure 2: Rover Concept 2

Concept 3 seen in Figure 3 is a four wheeled rover with a central motor and a gear drive. It is steered by a central steering servo for the two front wheels. The power is generated by an internal KRUSTY RTG. It has a hitch connector for a station to connect to.

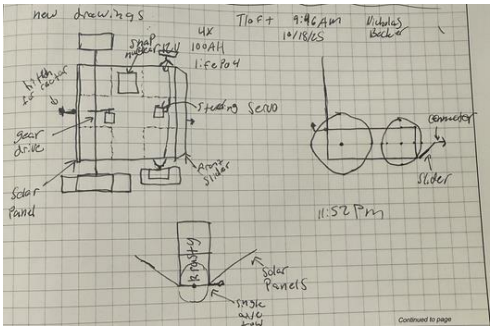


Figure 3: Rover Concept 3

Concept 4 seen in Figure 4 is a four wheeled rover, powered by four solar panels mounted above the rover and extending out over the wheels. This rover is driven by a traditional drivetrain and differential centered between the front two wheels. It also has a robotic charging arm on the rear side next to a hitch. The hitch will allow the rover to back up in front of the station, connect to the station, and pull it to a new desired location. Without a Multi-Mission RTG (MMRTG), it has four larger batteries storing power in addition to the four solar panels above the rover.

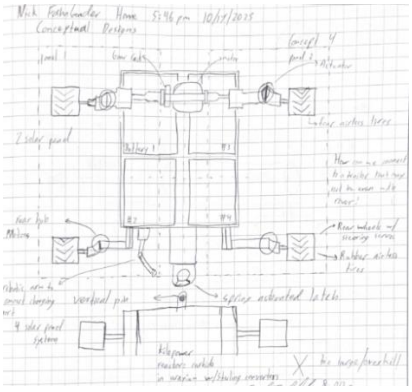


Figure 4: Rover Concept 4

Concept 5 seen in Figure 5 is a six wheeled rover utilizing a front bogie and rocker arm assembly to provide suspension to an MMRTG and single solar panel powered rover. This rover is driven by six hub motors and six servos to provide ground translation and steering. Again, this rover uses a robotic charging arm to detect and connect to a station, able to be hitched and trailered to a new desired location.

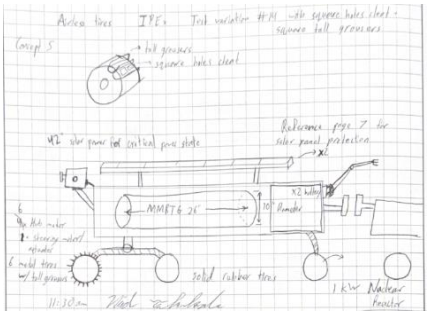


Figure 5: Rover Concept 5

Concept 6 seen in Figure 6 is a four wheeled four solar paneled rover with no suspension and a robotic charging arm. This concept is designed for an immobile station. With four solar panels mounted on adjustable side panels, the estimated power generated by the solar panels operating at near peak efficiency would be enough.

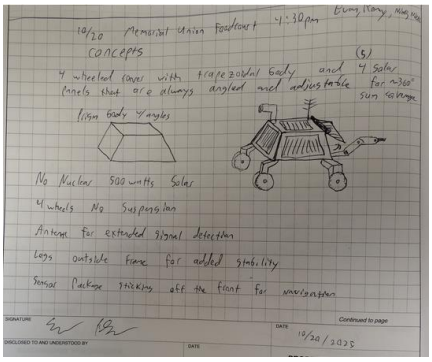


Figure 6: Rover Concept 6

Concept 7 seen in Figure 7 utilizes the rocker arm and bogie suspension system commonly applied to six-wheel rover designs. With a solid stick charging arm, it is designed to more simply and durably translate power generated by a single solar panel and MMRTG to and from other rovers and stations. The top solar panel is levered at the front end to allow for it to be tipped up to create a direct path of sunlight to the face of the panel.

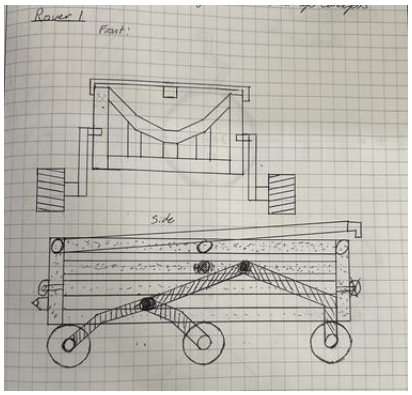


Figure 7: Rover Concept 7

Concept 8 seen in Figure 8 is another six wheeled rover taking advantage of the rocker arm and bogie suspension system. All six wheels are powered by hub motors, and four wheels are designed with steering motors. This design includes a trailer hitch on one end of the rover to pull a station from one location to the next, while the other end of the rover has a robotic charging arm to connect to a charging port on a station or other rover.

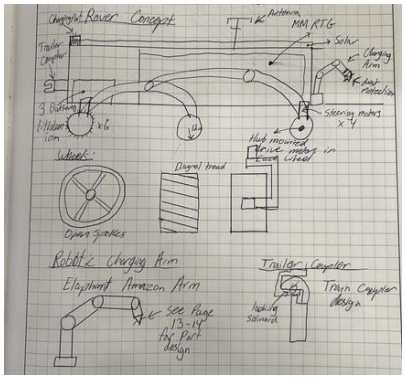


Figure 8: Rover Concept 8

Concept 9 seen in Figure 9 displays both the rover and station. The station is designed as a drive in enclosure with ramps to guide the rover into a certain position, aligning the male and female ends of the charging connection together. The rover has a consolidated body with no solar panels and an eight-wheel drive system.

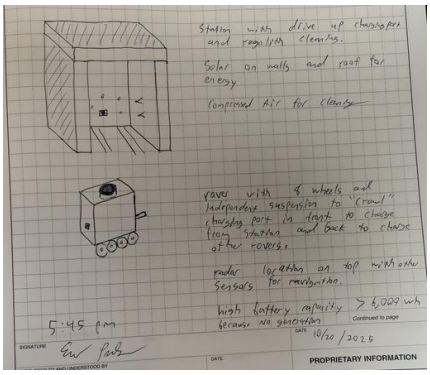


Figure 9: Rover Concept 9

Concept 10 seen in Figure 10 is the NASA Power Rover 1.0 previously created by NDSU senior design teams in 2021.



Figure 10: Rover Concept 10 - Power Rover 1.0

Following the creation of these 10 concepts, a screening matrix was developed to funnel out the subsystems that were estimated to perform poorly and create problems in the product development. On the contrary, the best systems used in these 10 concepts were picked out and made evident in the matrix. Taking the best systems from these concepts, three new concepts were made by combining appropriate and complimentary subsystems. Concept 8 did so well in the screening matrix that it was left untouched and taken into the next phase, being the scoring matrix. Figure 11 shows the concepts that were used to make new combinations as well as the concepts that were unused.

	Concept Propsed									
Selection Criteria	1	2	3	4	5	6	7	8	9	10
Power Storage Capacity	0	0	0	+	0	0	0	+	+	-
Power Transfer Rate	0	0	0	0	0	0	0	0	0	-
Power Generation Rate	0	+	0	-	+	-	0	0	-	-
Power Transfer Efficency	0	0	0	0	0	0	0	0	0	-
Weight of Rover	+	-	0	+	-	+	+	-	-	-
Minimum Speed	+	-	0	0	0	+	0	0	-	+
Turn Radius	0	+	0	+	0	-	0	+	-	0
Frame Clearance	0	-	0	0	0	-	+	+	-	0
Wheel Size	+	-	0	0	0	-	0	+	0	-
Suspension	+	0	0	-	+	-	0	-	+	+
Power Consumption Rate	0	-	0	0	0	+	-	+	-	0
G Force resistance	+	0	0	0	0	0	-	+	+	0
IP Rating of Components	0	0	0	0	0	0	+	0	0	-
Rover dimensions	0	0	0	0	0	+	-	-	0	-
Charging interface	-	0	0	0	0	+	+	+	0	-
Controller system	0	0	0	0	+	0	-	0	+	-
Station Mobility	-	+	0	+	0	-	-	+	-	-
Sensing capabilities	0	0	0	0	+	+	-	0	+	0
Steering	-	+	0	+	+	-	+	+	-	-
Drive Train	0	+	0	0	0	-	0	+	0	0
Sum +'s	5	5	0	5	5	6	4	10	5	2
Sum 0's	12	10	20	13	14	6	10	7	7	6
Sum -'s	3	5	0	2	1	8	6	3	8	12
Total Score	2	0	0	3	4	-2	-2	7	-3	-10
Continue?	NO	NO	Combine	Combine	Combine	Combine	Combine	Yes	Combine	NO

Figure 11: Rover Screening Matrix

Once the screening matrix was completed, drawings were made for three new concepts that were developed based on the combination of desirable features from the 10 initial concepts, as shown below.

Combination 1 seen in Figure 12 exemplifies a six-wheeled rover utilizing the bogie and rocker arm suspension system along with a solid stick charging port. The power generated on the rover is done by an MMRTG mounted inside the body of the rover, as well as two solar panels. One panel lays flat on the top of the rover, and the other panel lays at an angle down the back face of the rover. Both panels are protected by a film roll that is continuously pulled across the top and back face of the rover by a single motor.

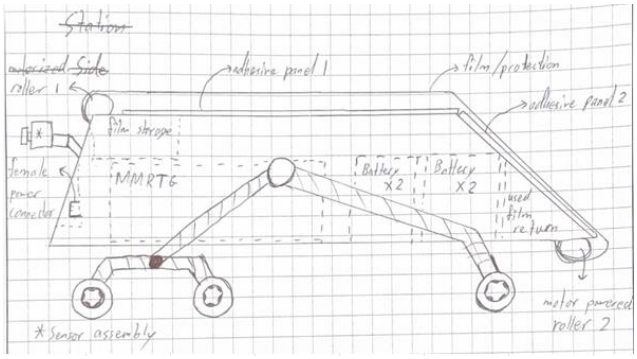


Figure 12: Rover Combination 1

Rover combination 2 seen in Figure 13 uses the same rocker and bogie suspension system that combination 1 uses. However, this next combination has four solar panels providing even more power. One panel on the top, one on each side of the rover, and one on the front. The charging port is also mounted on the other side of the suspension system, allowing for comparison to determine an optimized drive system.

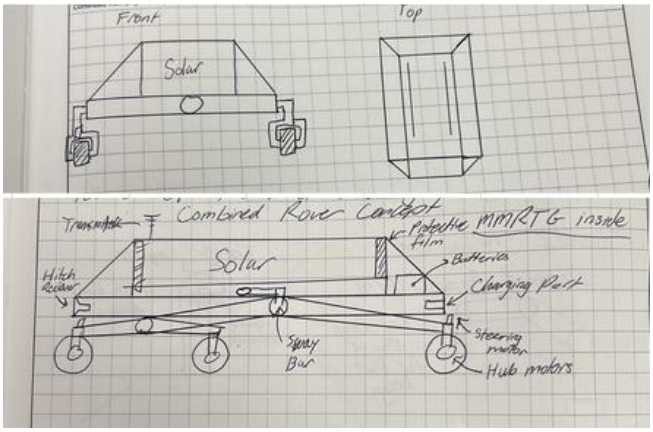


Figure 13: Rover Combination 2

Combination 3 seen in Figure 14 was more influenced by the rover and station concept that uses a drive in station with a ramp. This concept has eight-wheels with individual spring suspension. A solar panel that can be adjusted and tipped in all directions to increase efficiency is mounted on top of the rover to provide an additional 200 Watts.

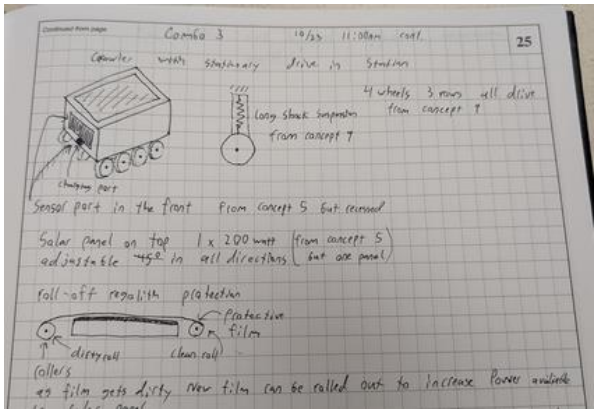


Figure 14: Rover Combination 3

Concept 8 seen in Figure 15 from the screening phase was unchanged and scored again using the new weighted matrix.

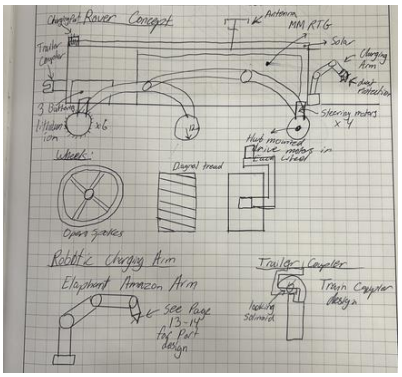


Figure 15: Rover Concept 8

Following a rigorous scoring matrix portrayed in Figure 16, the final design that was elected to be continued with was a rover combining several of the concepts and subsystems created by the four designs displayed in the scoring matrix. The selected rover uses a six-wheel rocker and bogie suspension system with a solid stick charging connection mounted on the front of the rover. It uses an MMRTG, three solar panels, and two batteries for power generation and storage. The rover is driven by six hub motors and four steering servos.

			Concept Propsed							
Selection Criteria	Weight	Relative W	8	Scores 8	Combo 1	Scores 1	Combo 2	Scores 2	Combo 3	Scores 3
Power Storage Capacity	8%	8%	3	0.24	3	0.24	3	0.24	3	0.24
Power Transfer Rate	8%	8%	2	0.16	4	0.32	3	0.24	3	0.24
Power Generation Rate	9%	9%	2	0.18	2	0.18	3	0.27	2	0.18
Power Transfer Efficency	5%	5%	2	0.1	3	0.15	4	0.2	5	0.25
Weight of Rover	4%	4%	2	0.08	3	0.12	3	0.12	2	0.08
Minimum Speed	6%	6%	2	0.12	2	0.12	3	0.18	2	0.12
Turn Radius	3%	3%	4	0.12	3	0.09	5	0.15	3	0.09
Frame Clearance	2%	2%	3	0.06	2	0.04	3	0.06	3	0.06
Wheel Size	5%	5%	2	0.1	3	0.15	4	0.2	3	0.15
Power Consumption Rate	8%	8%	2	0.16	2	0.16	2	0.16	1	0.08
G Force resistance	2%	2%	1	0.02	2	0.04	2	0.04	5	0.1
IP Rating of Components	4%	4%	3	0.12	2	0.08	3	0.12	4	0.16
Rover dimensions	4%	4%	2	0.08	3	0.12	4	0.16	3	0.12
Charging interface	7%	7%	2	0.14	2	0.14	4	0.28	2	0.14
Controller system	5%	5%	3	0.15	3	0.15	3	0.15	3	0.15
Station Mobility	5%	5%	2	0.1	2	0.1	2	0.1	0	0
Sensing capabilities	4%	4%	1	0.04	2	0.08	4	0.16	3	0.12
Steering	6%	6%	3	0.18	3	0.18	5	0.3	2	0.12
Drive Train	5%	5%	4	0.2	3	0.15	4	0.2	3	0.15
	100%									
	Total		Score 8:	2.35	Score 1:	2.61	Score 2:	3.33	Score 3:	2.55

Figure 1616: Rover Scoring Matrix

Figure 17 below shows the selected concept, combination 2 that would be refined and finalized in the detailed design portion of the project.

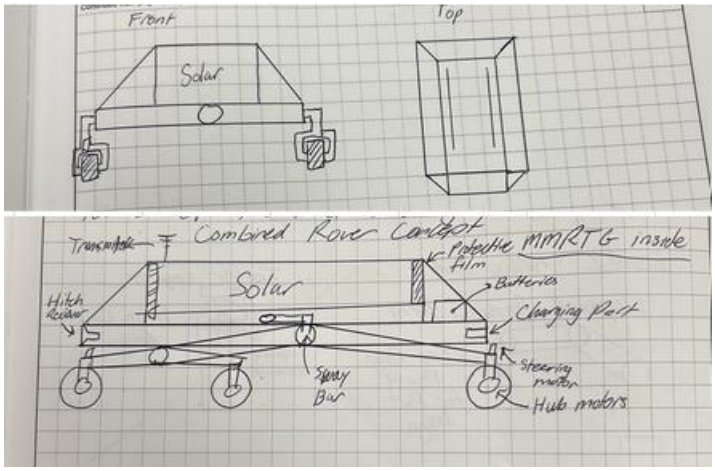


Figure 1717: Selected Rover Concept

Station Selection

The development of the charging station required careful consideration of multiple designs. The primary function of the station is to serve as a high-capacity energy hub capable of storing substantial amounts of power. It also must be able to recharge quickly in order to service multiple rovers as operations become larger. This stored energy must be readily available to rapidly and efficiently recharge rovers operating within a reasonable radius. Achieving this objective requires an initial analysis of many different power generation methods. Given the station's role, it was essential that the energy harvesting system be highly effective and capable of producing consistent power under expected and unexpected environmental conditions.

Another major design consideration involved determining whether the station should be mobile, semi-mobile, or completely stationary. Several configurations were evaluated, including the possibility of a movable structure or a trailer-based system. However, an examination of established mission strategies revealed that NASA typically deploys such infrastructure in predetermined optimal locations. These sites are chosen to maximize solar exposure and to support the greatest number of rover operations.

Based on this understanding, a fixed, immobile station was determined to be the most efficient solution. This choice eliminated unnecessary weight, reduced mechanical complexity, and minimized potential points of failure associated with mobility mechanisms. By reducing system complexity and focusing on reliability and energy capacity, the final design supports long-term performance and dependable power delivery for rover charging operations.

Station concept 1 seen in Figure 18 for the station is a non-mobile design, meaning it is placed once by a NASA launch vehicle in an ideal location and remains there for the entire mission. This concept uses an RTG as the primary power source and eliminates solar panels to reduce overall weight. It also incorporates a robotic charging arm capable of connecting to any rover operating in the surrounding area.

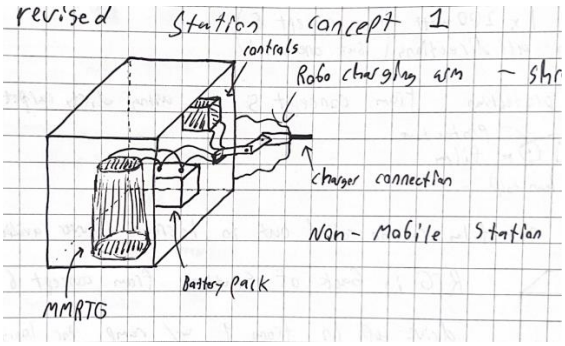


Figure 1818: Station Concept 1

Station Concept 2 seen in Figure 19 is a garage style station with an internal stick charger and alignment grooves in the floor to ensure the connection is made properly. The power is generated by solar panels on the sides and roof of the station. The inside of the station includes devices that can clean regolith off of the rover especially regolith off the rover solar panels.

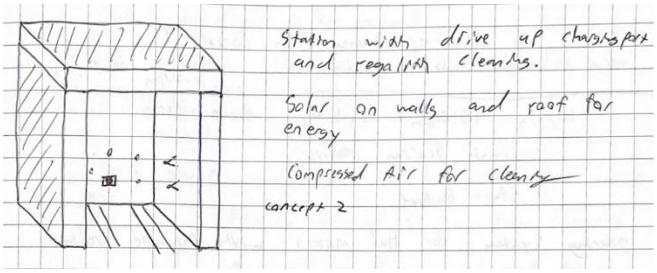


Figure 1919: Station Concept 2

Concept 3 seen in Figure 20 is an immobile station that uses both an RTG and folding solar panels to provide power generation. This hybrid approach increases total energy availability while maintaining a fixed deployment location for simplicity and reliability.

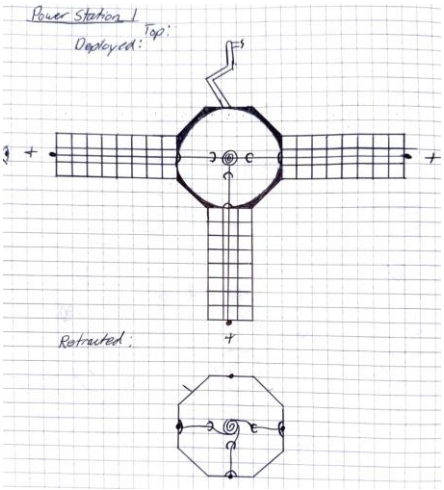


Figure 2020: Station Concept 3

Station concept 4 seen in Figure 21 is a trailer style station that connects via train coupler to the rover and can be relocated, wheel locks keep the station in place while the rover is disconnected. It has a robotic charging arm that autonomously connects to rovers to charge them. Actuating solar panels and an RTG provide power for the station.

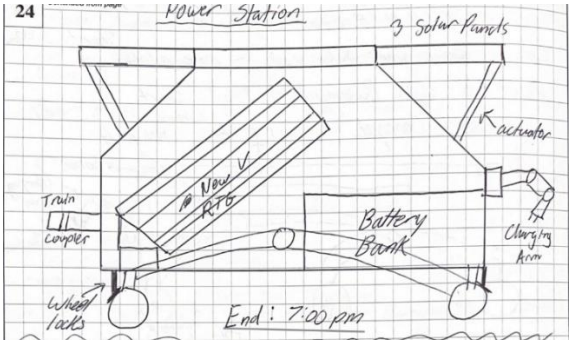


Figure 2121: Station Concept 4

Concept 5 seen in Figure 22 is a lightweight trailer-style station designed to be towed behind the rover, allowing continuous charging while the rover is exposed to sunlight. The design prioritizes low mass and minimizes moving parts to enhance reliability and reduces mechanical complexity.

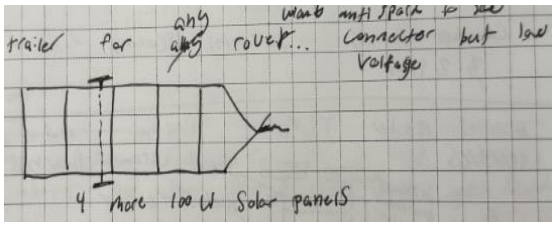


Figure 2222: Station Concept 5

	Concept Propsed				
Selection Criteria	1	2	3	4	5
Ability to Connect with Rover	0	0	0	0	-
Ability to Transfer Power to Rover	0	0	0	0	0
Weight	0	-	-	-	+
Ability to Relocate	0	0	+	+	+
Regolith Protection of Connection	0	+	0	0	0
Power Storage	0	0	0	0	-
Power Generation	0	-	+	+	-
Additional Rover Interactions	0	+	0	0	+
Station Regolith Resistance	0	0	0	-	-
Ability to Connect with multiple Rover sizes	0	-	0	0	-
Sum +'s	0	2	2	2	3
Sum 0's	10	5	7	6	2
Sum -'s	0	3	1	2	5
Total Score	0	-1	1	0	-2
Continue?	Combine	Combine	Yes	Combine	Combine

Figure 2323: Sation Concept Screening

The station concepts were screened with the screening matrix shown above. The criteria are largely based around charging the rover and collecting energy on mars as those are the two major functions needed for the station to meet its objective. Concept 3 had the highest score out of the five concepts so it was selected to move on. All stations were combined into two additional combinations to score as well.

Combination 1 seen in Figure 24 incorporates elements from both Concept 2 and Concept 1. From Concept 2, it uses a garage-style design, allowing the rover to drive inside the station to protect the charging ports from regolith contamination. From Concept 1, it adopts the RTG as a power source, enabling continuous battery charging regardless of solar exposure.

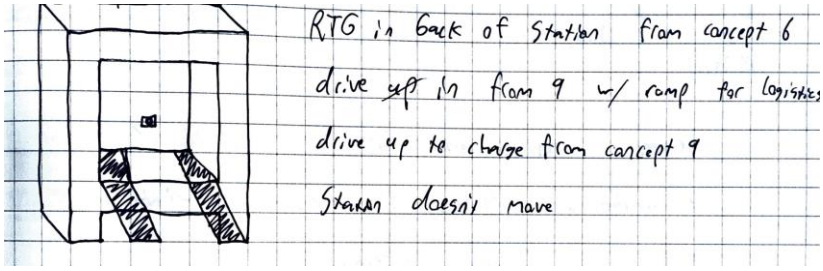


Figure 2424: Station Combination 1

Combination 2 seen in Figure 25 uses components from concept 1, concept 2, and concept 3. Concept 1 has the RTG for power generation, Concept 2 has the stick style charger with alignment ramp, and concept 3 has the body style and the three actuating solar panels.

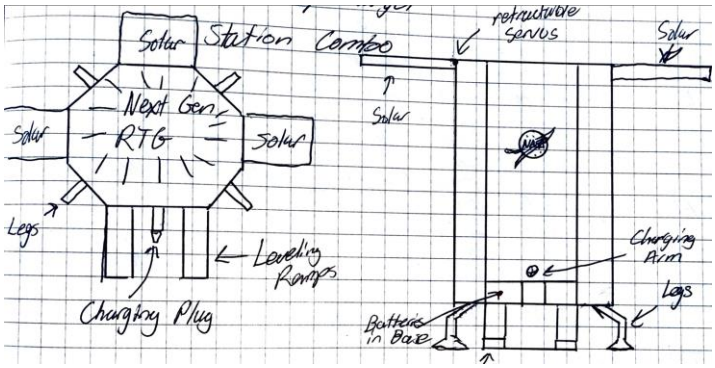


Figure 2525: Station Combination 2

			Concept Propsed					
Selection Criteria	Weight	Relative W	Concept 3	Scores 3	Combo 1	Scores 1	Combo 2	Scores 2
Ability to Connect with Rover	15	0.15	8	1.200	7	1.050	7	1.050
Ability to Transfer Power to Rover	10	0.10	7	0.700	7	0.700	7	0.700
Weight	5	0.05	4	0.200	5	0.250	6	0.300
Regolith Protection of Connection	10	0.10	3	0.300	8	0.800	6	0.600
Power Storage	15	0.15	6	0.900	4	0.600	8	1.200
Power Generation	10	0.10	8	0.800	5	0.500	9	0.900
Additional Rover Interactions	3	0.03	0	0.000	6	0.180	0	0.000
Station Regolith Resistance	8	0.08	5	0.400	5	0.400	5	0.400
Ability to Connect with Multiple Rover sizes	9	0.09	8	0.720	3	0.270	2	0.180
Durability During Takeoff and Landing	9	0.09	6	0.540	8	0.720	8	0.720
Communication with Rovers and Earth	6	0.06	6	0.360	6	0.360	6	0.360
	100		Total:	6.120	Total:	5.830	Total:	6.410

Figure 26: Station Concept Scoring

The screening process used the screening matrix shown above. The criteria weighed the heaviest are the ability to connect with the rover, and the power storage. These criteria emphasize the objective to autonomously charge a rover. The other important criteria are power transfer rate, regolith protection, and power generation. These criteria also are critical to the mission of charging a rover.

After assigning scores based on the ability of each station to meet the criteria. The relative weights are multiplied by the scores to get a weighted score, the weighted scores are summed at the bottom to compare the suitability of the concepts for the required objectives. Combination 2 was the winner and the concept selected to advance to design analysis.

Detailed Design Documentation

Motor Selection

The first design constraint that needed to be determined was the type of motor to use to physically move the rover. There are a wide variety of motors capable of driving a rover. The largest issue that needs to be solved when choosing the motor is that it can perform reliably under the conditions and requirements of the mission. Several options were considered, including brushless hub, brushless DC in-runner, brushless DC out-runner, and brushed DC motors. Brushless hub motors are simple, quiet, and low maintenance because the motor is built directly into the wheel, this allows for the possibility to eliminate the use of belts or chains. Unfortunately, this type of motor adds rotational mass, and is often more prone to overheating due to limited airflow. Brushless DC in-runner motors are compact, highly efficient, and capable of high RPM, making them ideal for gear-driven systems, but they produce relatively low torque at low speeds and typically require a gearbox or reduction system to be practical in the use of a rover. Brushless DC out-runner motors provide strong low-RPM torque, smooth acceleration, and effective cooling thanks to their spinning outer shell, but the exposed rotor can collect debris which would happen very quickly in the Martian environment. They are also more easily damaged and introduce extra vibration. Brushed DC motors are inexpensive, easy to control, and provide strong startup torque, but their brushes wear overtime, generate friction and electrical noise. This results in lower efficiency and durability compared to that of the modern brushless

designs. After extensive research, hub motors were selected for their high reliability and near-zero maintenance requirements.

Solar Protection

The next aspect examined was how to protect the solar panels from the large amounts of regolith blown across the surface of Mars. The first protection concept involved placing a hard glass layer over the solar panel, allowing a scraper to push regolith off without damaging the cells. This required research into the composition of Martian regolith and whether a glass strong enough to resist scratching could be manufactured without significantly reducing the amount of sunlight reaching the panel. Martian regolith is heavily based on basalt, which has a Mohs hardness of about 6. Modern Gorilla Glass typically falls between 6 and 7 on the Mohs scale, which seemed too close to provide reliable protection. This led to exploring sapphire glass as an alternative. Although more expensive, sapphire glass has a Mohs hardness of 9, providing sufficient durability to maintain a clean and clear protective layer, ensuring maximum solar energy transmission.

The second concept that was created was the use of a conveyor belt style film protection that would wrap lengthwise around each of the solar panels individually. This would allow for a clear, flexible protective film to be rotated around the solar panel in a fixed loop. This loop would be collecting the regolith and dust while facing outwards, then being cleaned off as it rotates on the inside face of the solar panel frame assembly it is fixed to. This was a good solution; however, it would require a complicated assembly set up underneath the frame to clean the regolith and dust off the film. The cleaning assembly would have included a number of large parts and complex mounting systems, ultimately taking up valuable budget and space on the inside of the rover.

Another solar protection method considered was the use of tear-off and roll-off films. This idea was inspired by motocross, where similar systems keep goggles clear even in muddy conditions. The concept is simple: when a layer of film becomes too dirty, a thin sheet of plastic is pulled away, exposing a clean layer underneath. This allows multiple layers without the need to scrape debris across a hard surface. Roll-offs were ultimately chosen because they provide a reliable way to expose a fresh, unscratched layer at any time, without relying on glass that could potentially crack, scratch, or fail during transport or while on the Martian or lunar surface. As the designing progressed, this idea was taken and combined in the concept of screening and scoring phases to become a continuous roll of film that would be fed from a roll source, wrapped around the solar panel and frame, pulled around a dual roller motorized assembly, and finally collected in a film return tray. This design, seen in Figure 27, utilizes a motorized roller assembly that relies on springs to compress the film between two rollers, one that is powered and turned by a motor through a 1:1 gear configuration.

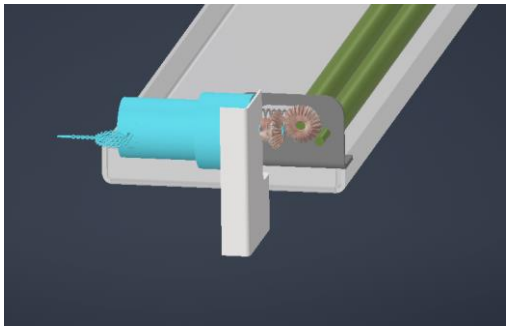


Figure 27: Selected Film Assembly

Roller Motor

One of the major components in the assembly shown in Figure 1 is the motor. To pull the protective film off the roll, over the length of the solar panel, around the top edge of the aluminum sheet, and back down through the dual roller system, a motor with sufficient torque would be necessary. To determine the force that would be created by the contact in addition to the desired slack force on the free side of the motorized roller, the following equation was solved using a series of values.

$$F_{friction} = F_{tension} e^{\mu\theta}$$

The equation shown above used a desired tension load of 15 lbf. This is intentionally high because this will cause the film to be pulled tightly across the solar panel. This will minimize regolith and dust from getting between the film and the solar panel, in addition to preventing a windstorm from blowing the film away from the solar panel. Another estimation used in this calculation is a coefficient of friction of 0.2 between the aluminum sheeting and the plastic film along the top edge of the sheeting. The friction force created in this configuration due to the tension force was 28.11 lbf.

$$T = F_{friction} r$$

Once the frictional force was found, the required torque of the motor was calculated using the equation above. The radius of friction that the torque must overcome was found to be 0.25 inches. By multiplying this by the friction force, the required torque of the motor was found to be 112.4 in-oz. With this metric found, a motor with a shaft size of 0.25 inches was selected from McMaster-Carr that has a higher maximum torque than this.

Bevel Gear

The next component that needed to be selected was the gear by which the shaft would be turned. With limiting spatial constraints, a bevel gear configuration was necessary to form a 90-degree angle between the motor and the rotating shaft. To make this selection, a simple moment calculation was made to determine the force that this gear would undergo due to the input torque of the motor. To find the transmitted load of the motor onto the bevel gear, the torque is divided by the average radius of the gear.

$$W_t = \frac{T_i}{r_{ave}}$$

By dividing the selected motor torque of 7.025 in*lbf by the average radius of the bevel gear, found to be 0.45 inches, the force acting on the end of the bevel gear was 15.61 lbf. Despite being higher than expected, the maximum transmitted force allowable of the selected bevel gear is 75 lbf. The reason for the bevel gear being chosen and then verifying the force load was because of the spatial constraints limiting the selection to a minimal number of possibilities. Additionally, the maximum transmitted load of the gears were significantly higher than what will be created by the assembly.

Spring

The last major component of this sub assembly was the selection of a spring to compress the two rollers against each other to ensure that the film would be pinched by the two and pulled through efficiently. Similar to the last step, a spring was selected to fit the dimensions of the application first. Once the spring was selected calculations needed to be performed using the specifications of the spring to determine how far the spring would need to be compressed inside of the bracket. With a spring rate of 45 lbf/in and a maximum deformation of nearly half an inch, the spring force must be greater than that created by friction. The kinetic coefficient of friction between the protective film and the top edge of the frame was estimated to be $\mu_k = 0.2$. By solving the following equation for friction force, the minimum force required for the spring to overcome was determined.

$$F_{friction} = \mu_k N$$

By using the same 15 lbf from the previous calculation, the frictional force was found to be 3 lbf. With this value, the distance that the spring must be compressed was able to be found. By solving the following equation relating to this force and the spring rate, the distance was determined.

$$F = xk$$

The frictional force was 3 lbf, and the spring rate, k, was 45 lbf/in, thus giving a value of 0.067 inches for the spring to be compressed at the very minimum.

Main Controllers

The selection of the main controller was another very important aspect of the rover's design. The main controller is arguably the most important component in the entire rover. This is because it manages every function of the rover, including steering, driving, and sensor control. Therefor choosing a compatible and extremely capable controller is essential. One common option is a basic microcontroller, such as an Arduino. Using an Arduino offers advantages such as low cost and simplicity. Another benefit of using an Arduino is the access to a large amount of community support. This makes programming and troubleshooting relatively simple since related projects have been done. Arduinos are lightweight, energy-efficient, and compatible with a wide range of sensors and motor controllers. This makes them suitable for small or educational rover projects. However, they have many notable limitations. Some of which include lack of processing power required for advanced tasks such as real-time image processing or autonomous navigation. They also have limited memory and lack built-in operating systems and redundancy features found in more robust and complex systems. As a result, while effective for basic control

and simple automation, a basic microcontroller becomes restrictive for larger or more complex, mission-critical rovers.

The next controller examined was an F405 controller. This type of controller is commonly used in drones and remote-controlled aircraft. It is highly regarded for its modular design and versatility. It provides access to advanced, well-developed firmware, which allows for extensive customization along with fine tuning of its operations. Compared to simpler microcontrollers, the F405 offers significantly greater processing power. It is also extremely capable of handling complex tasks with much higher efficiency and reliability. It supports advanced features such as precise position tracking, sensor fusion, and real-time motor control. While using a basic controller, such as an Arduino would make these tasks difficult or nearly impossible to implement effectively. Additionally, its compatibility with a wide range of sensors and cameras makes it an ideal choice for sophisticated systems that require very high levels of responsiveness and coordination. Overall, the F405 controller offered far greater capability for a complex rover system, providing flexibility and performance necessary for advanced operations. Although it does come with added complexity in setup, programming, and configuration for a project this important which makes it worth it.

Servos

The servos serve as a critical subsystem within the rover, as they provide the sole mechanism for steering. The rover utilizes a total of four servos arranged in a series configuration, allowing each wheel to rotate appropriately during turning maneuvers. Proper servo selection required a detailed analysis of the mechanical loads encountered during operation, especially the torque needed to overcome the normal force and friction acting on each wheel.

$$F_{friction} = \mu_k N$$

To determine the required servo specifications, the expected weight distribution across all four wheels was calculated. Combined with the estimated coefficient of friction between the wheel material and the terrain, these values provided the torque threshold necessary for reliable steering. The steering angle requirements were then evaluated to ensure adequate maneuverability. A 270-degree servo configuration was selected to permit mechanical gearing, which increases available torque and enhances steering control.

$$T_{out} = T_{in} \frac{R_{output}}{R_{input}}$$

Based on the completed calculations, high-torque servos rated at 160 kg·cm were chosen to ensure dependable operation under all expected loading conditions. This selection provides a safety margin and supports consistent performance across both varied terrain and mission scenarios.

Frame

Another critical component of the body of the rover was the base level of the frame. This level of the frame plays the crucial role of mounting the top body including all its components, framing, and subassemblies of the rover onto the supporting suspension system. Analysis of the frame was done to ensure that the forces created by these components do not cause deflection and stress that will compromise the rover and its ability to navigate lunar and Martian surfaces.

The first image below shown in Figure 28 displays the stress created by the components previously mentioned, namely, the four vertical 1x1 aluminum tubes, the solar panels and supporting aluminum sheeting, the electrical components, the solar protection assemblies, and lastly the MMRTG. This simulation accounts for a worst-case scenario load developed by an overestimate of the black-boxed MMRTG as well as the electrical components. Because of lead times and available stock varying, to ensure that the frame could withstand the stress, an exaggerated distributed load of 100 lbf was placed over both the front and rear storage compartments. This load was also determined to absorb any conduits and wire routings that are added to protect all electrical components, in addition to the batteries, which will make up a large portion of that load.

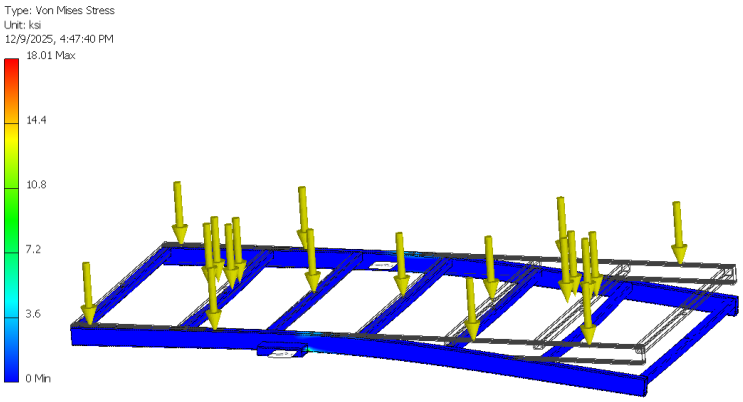


Figure 2827: Stress Developed in Rover Frame

With the loads and constraints set in place, the maximum stress that was developed in this configuration came out to be 18.01 ksi. This maximum stress accumulated at the weld of the shoulder joint and the lengthwise supports of the frame. The shoulder joint is a 1x2x1/8-inch tube that will fix the frame onto the suspension mount bearings. Again, this is a worst-case scenario as most of the electrical components will be placed in the front storage compartment which will both bring more of the weight closer to the suspension mounting point as well as making the center of gravity closer to be directly above the frame on suspension mounting point.

Figure 29 displays the displacement of the base level of the frame under the described load. Due to the mounting point towards the front of the rover and a large load towards the rear of the rover, the displacement came out to roughly a quarter inch. This will be reduced by both locating more of the electrical components towards the front of the rover, and the use of lengthwise supports connecting the front vertical tubes to those at the rear.

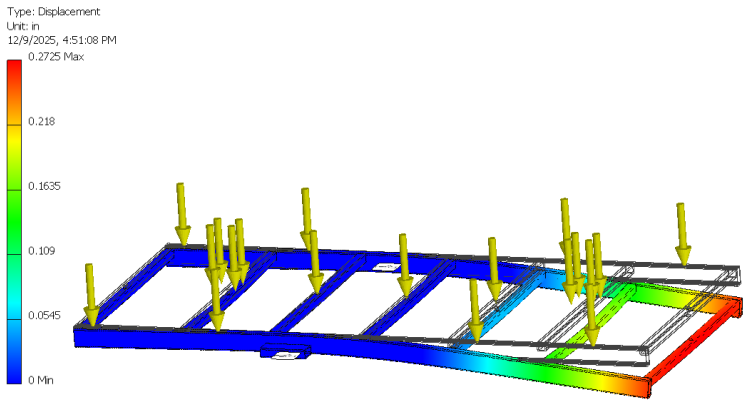


Figure 2928: Deflection Created in Rover Frame

Figure 30 below shows a simulation ran with similar loads but with the rest of the rover frame included. The displacement created in this simulation is closer to half of what was created by the base level frame only model. Both were ran to clearly portray the maximum deflection and stress created by the design.

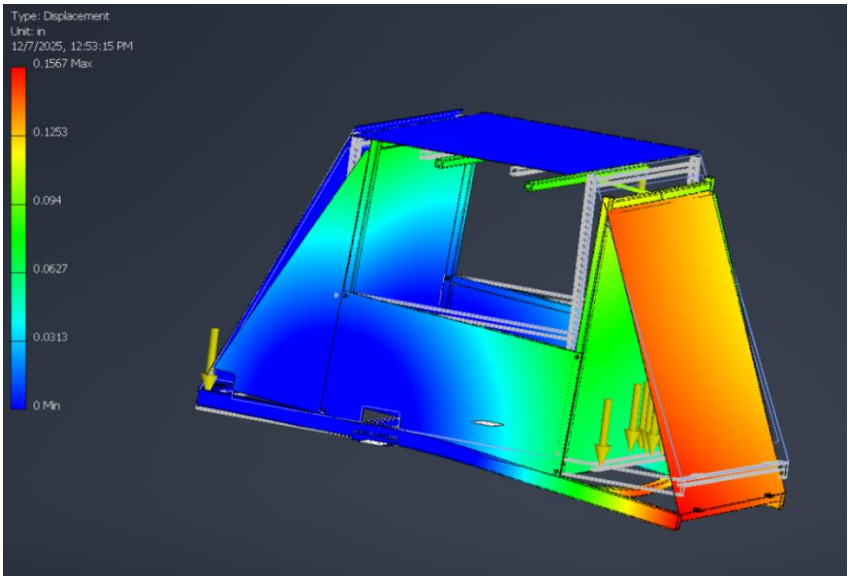


Figure 3029: Entire Rover Frame Displacement

Suspension Assembly

The suspension system is a critical component of the rover, as its performance directly influences overall efficiency, traction, stability, and climbing capability. The selection process for the suspension involved many key considerations. An initial estimate of the rover's operating speed was first required to determine whether damping elements, such as springs or shock absorbers, were necessary. This would be in order to prevent excessive bouncing during motion. After evaluating expected travel speeds, it became clear that the rover would move at relatively low velocities. This means that the need for traditional suspension components is not necessary for this design.

After reviewing numerous existing rover designs, this idea was confirmed. Most comparable systems lacked springs or damping mechanisms due to their minimal operating speeds. This observation led to a focused examination of rocker-bogie-style suspension system. This type of suspension system is commonly used in planetary exploration rovers. The rocker assembly was studied to understand the mechanics behind its ability to maintain stability, distribute loads, along with being able articulate over uneven terrain without relying on conventional suspension elements. Due to its popular use among NASA and the stability this suspension design provides, the rocker-bogie suspension system was selected for the final design.

This suspension system is composed of three major parts. The rocker arm attaches to a pivot point on the frame and set forward from the center of gravity. The front of the arm spans down to the front wheel assembly while the rear spans down to the pivot of the bogie arm. The bogie arm then spans forward and down to the central wheel while the rear spans down to the rear wheel. The rocker arm has a vertical offshoot that attaches to a central differential pivot arm that attaches the two sides of the suspension together. This system allows for articulating movement of each side of the rover while maintaining distributed balance between all six wheels.

The design of this system was created so that the top of the wheels would have 6 inches of vertical travel before reaching the bottom of the frame. This was determined to be sufficient height for any terrain this rover would endure. To ensure that a wheel contacted terrain before the frame did, the suspension spanned horizontally so the position of the axles of the front and rear wheels would align with the ends of the 64-inch rover frame. The rocker pivot sits 8 inches in front of the center of gravity where it is attached via pivoting linkages. This 8-inch offset to the differential allows optimized wheel load distribution while maintaining a safe load on the center pivot. It was determined that aluminum 6061 would be used due to its high strength, light weight, and low cost. This is the designed structure of the rocker-bogie suspension system which was analyzed and tested under a load of 300 lbf per side to represent the rover in maximum conditions. To determine the dimensions of the arms themselves, the following equations were used:

$$\text{Bending Stress: } \sigma = -\frac{My}{I}$$

$$\text{Area Moment of Inertia (square): } I = \frac{bh^3}{12} = \frac{h^4}{12}$$

Using the yield strength of aluminum 6061 under a factor of safety of 1.4, an allowable stress of 25 ksi was determined for the suspension arms. Under maximum loading conditions, one side of the system would have a load of 300 lbf. For the rocker system, this implies the front wheel having to withstand a force of 100 lbf vertically and the back connection to the bogie arm facing a 200 lbf force (assuming equal wheel distribution). Using the moment created by the 200 lbf and the distance to the rocker pivot along with the area moment of inertia, the dimensions of the square bar stock was determined to be 1.03 inches minimum to achieve a factor of safety of 1.4. For manufacturing purposes, a common sized bar stock of 1.25 inches was chosen for the design while staying above the dimensions of 1.03 inches. To reinforce these calculations and ensure safe operations, FEA simulations were run on both the rocker and bogie arm. These simulations are detailed in Figure 31 and Figure 32 below.

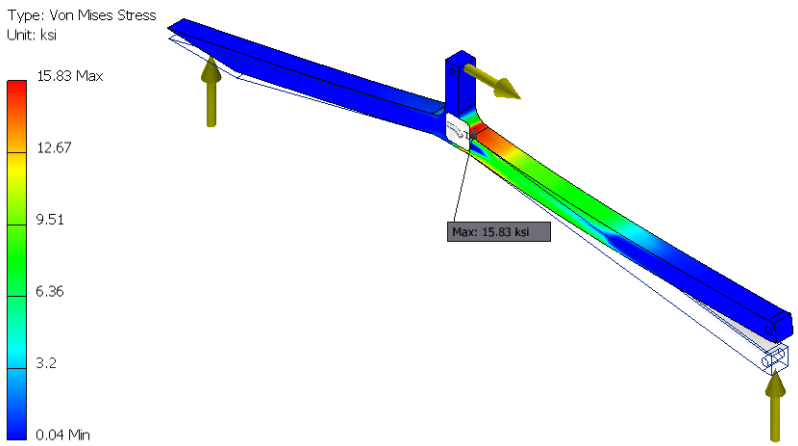


Figure 3130: Rocker Arm FEA Simulation

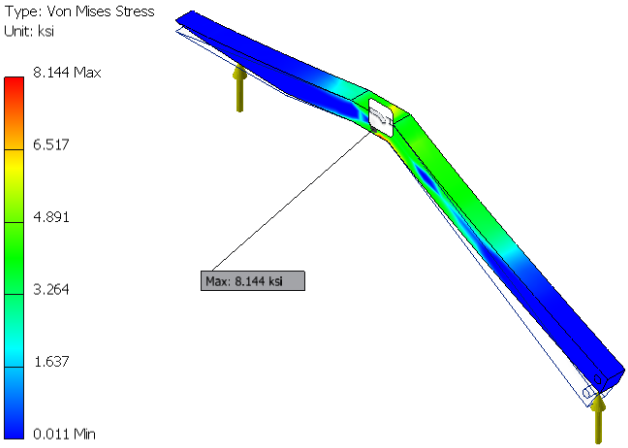


Figure 3231: Bogie Arm FEA Simulation

The results of these simulations proved that under maximum conditions, the 1.25-inch square aluminum bar stock chosen for this design reached a max stress of 15.83 ksi, a max deflection of 0.43 inches, and had a factor of safety of 2.29 which meets all required design criteria. This maximum stress and deflection occur in the longer rocker arm, but the bogie is lower due to its smaller size assuming the two components are made of the same material for ease of manufacturing.

The same analysis was performed on the center differential arm to determine if the same material would work. Using the same calculations used prior, the dimensions of the cross section needed to be larger than 1.32 inches of square bar stock aluminum. This is larger than the chosen size of 1.25 inches for the suspension components, so a bar stock size of 1.5 inches was selected which gave a factor of safety of 2.05, surpassing the 1.4 requirement. FEA simulations were once again run to confirm calculations and the results below in Figure 33 show that this size will work for the application.

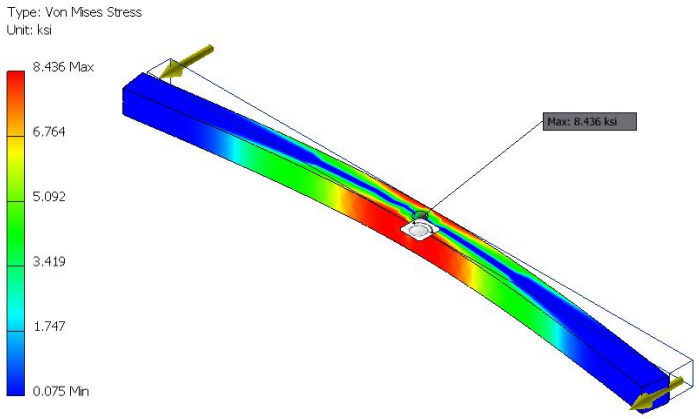


Figure 3332: Center Differential Arm FEA Simulation

All linkages and bolts used in this assembly were chosen based on load ratings provided by manufacturers using the maximum load criteria detail previously. Sizes of these components may have ran larger in cases that required pin alignment to help mitigate slop in the system. Cost factors were also taken into consideration when selecting these purchased parts.

Wheel Assembly

Hub motors were selected before the detailed design of the surrounding components of the wheel assembly to ensure a system that integrated seamlessly with the profile of this motor. Based on the ratio of wheel size to frame size of previous NASA rovers being 0.17-0.2, a wheel diameter of 12 inches was selected for the 64-inch rover frame. The chosen material for these wheels was 3D printed TPU for fast, customizable manufacturing paired along with flexible characteristics to provide additional traction and shock absorption.

The motors that were selected have a dual prong mounting design with studs protruding off either side of the hub. This profile governed the design of the wheel mounting bracket so that the wheel is attached on both sides to not overload the studs. Calculations were then performed to determine the thickness that the bracket needed to be. This was determined by the top of the plate where the most bending stress occurs under a load. Stainless steel 304 was the selected material for this bracket instead of aluminum due to its high strength while being easy to work with. This plate will also be attached to the steering shaft which is planned to be stainless steel as well due to its higher modulus of rigidity. The allowable yield strength of Stainless Steel 304 with the 1.4 factor of safety is 21.43 ksi. This plate needed to be 5.5 inches wide to account for the width of the wheels and 1.25 inches wide to attach to the designed steering shaft to be described later. The thickness of the plate was determined through the following calculations:

$$\text{Bending Stress: } \sigma = -\frac{My}{I}$$

$$\text{Area Moment of Inertia (rectangular): } I = \frac{bh^3}{12}$$

Under maximum conditions of 100 lbf per wheel previously described, the h value (thickness of the plate) was determined to be a minimum of 0.18 inches. Moving to the next available stock size, 3/16-inch Stainless Steel 304 plate was chosen for the design.

Attached to the plate is the steering shaft combined with a thrust bearing housing. This shell is designed to be recessed into the mounting plate attached to the suspension arms. This allows for regolith protection for the bearing while still allowing rotational movement. The shaft diameter was determined through the following calculations:

$$\text{Maximum Allowable Shear Stress: } \tau_{allow} = 0.577\frac{\sigma_y}{FOS}$$

$$\text{Shear Stress: } \tau = \frac{Tr}{J}$$

$$\text{Polar Moment of Inertia (Round Shaft): } J = \frac{\pi d^4}{32}$$

Using the allowable yield stress of 21.43 ksi for Stainless Steel 304, the allowable shear stress was determined to be 12.36 ksi. The torque the shaft will experience was governed by the maximum torque of the steering servos which was found to be 138.87 in*lbf. After combing the equations above, the diameter of the shaft based on the given criteria can be found through the following formula:

$$\text{Shaft Diameter: } d = \left(\frac{16T}{\pi\tau}\right)^{\frac{1}{3}}$$

The final diameter of the shaft based on quantities outlined above came out to 0.386 in. This is slightly above 3/8 of an inch so the next size chosen for the shaft was ½ inch diameter. This shaft size governed the size of other components to be used in the subsystem such as bearings. A thrust bearing and ball bearing were chosen based on an inside shaft diameter of ½ inch and all both are rated up to 1,900 lbs based on manufacturer specifications.

The aluminum plate that connects the suspension system to the wheel assembly is designed to mount the servo motor above the steering shaft where they will be attached with a shaft collar. This plate thickness is determined by the functionality of the recessed groove in which the thrust bearing housing sits. This design protects the bearing inside from regolith due to the overlap in geometry. The groove is 1/8 inch deep so the plate itself was made ¼ inch thick so that the groove would not cause failure in the structure. An FEA simulation was run on this plate to determine the maximum stress which came to be 14.71 ksi which is well below the allowable stress for aluminum. This simulation is below in Figure 34.

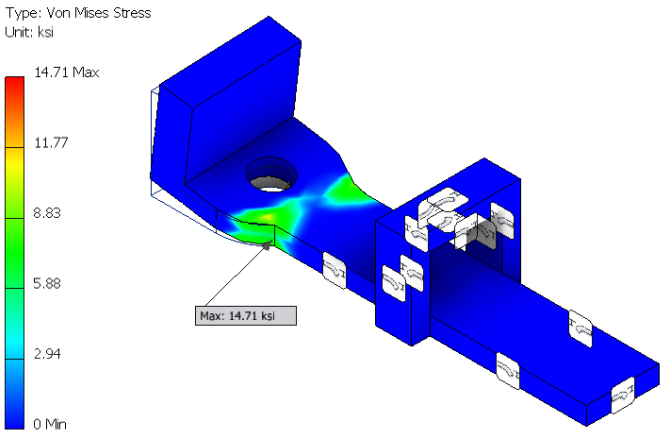


Figure 34: Wheel Mounting Plate FEA Simulation

Station

From the station selection process an immobile station was chosen with an external stick charger and a ramp for alignment. The station is raised off the ground on 5 legs to prevent drifting of regolith and to level the station as much as possible. There are three solar panels that need to collect 300 Watts of solar total. The components needed are: aluminum tubing for the frame, aluminum sheeting for the floor, walls, roof, and solar panel supports, foot pads, solar panels, batteries, solar controller, alignment ramp, and charging assembly.

The loads the station will experience are from the weights of the components. The high stress areas are where the solar panels create a moment on the bracket and frame, as well as the cross members where the RTG sits. The solar panel assemblies are 20 lbs each with the center of gravity at the geometric center of the 23in wide by 43in long solar panel. This creates two moments on the brackets perpendicular to each other, one bending moment of 430 in*lbs and another of 230 in*lbs both distributed over two brackets. The magnitude of the moment of each bracket becomes 243.8 in*lbs. To account for the weight of components acting on the member and any stress concentrations a total corrected bending moment of 300 in*lbs is used for hand calculations. The weight of the RTG and other components housed inside of the station is estimated at 1,200 lbs. To account for worst case scenarios the weight is distributed into the middle of the cross beams of the frame floor.

Using the bending stress equation with a maximum stress of 25 ksi using the factor of safety and a minimum yield strength of 35ksi for 6061 aluminum, a y of half the diagonal because the moment is applied approximately across the diagonal not across the flat side, and the I equation for square tubing $I = \frac{(s_o^4 - s_i^4)}{12}$ where $s_i = s_o - .0625$. Solving for the side length of the tubing $\frac{300 \cdot 1.41 \cdot s_o}{2 \cdot 25{,}000} = \frac{s_o^4 - (s_o - .0625)^4}{12} \Rightarrow s_o = .683in$ this is the minimum side length needed for the frame tubing. Rounding up to the nearest nominal size the tubing selected to build the frame is ¾" square tubing 1/16” thick made of 6061 aluminum.

The station frame was modeled using this tubing. The diagonal members are made of ½" square tubing 1/16” thick because they fit better for manufacturing and they carry less stress. Everything else is made of ¾" tubing for manufacturability. The sheeting for the sides is neglected for stress analysis because it is extremely thin and due to assembly might not carry loads anyways,

additionally a failure in the integrity of a side panel should not compromise the factor of safety for the overall frame. Using these parameters FEA analysis was run using Inventor's stress analysis. The results fo thei FEA analysis can be seen in Figures 35 and 36. The simulation yielded a maximum stress of 19.92ksi and a maximum deflection of ~0.5 inches. The maximum stress is used in the factor of safety equation to solve for the new minimum FOS = 1.77. This falls within NASA's requirements and confirms the accuracy of the original tubing calculations. The ½" of deflection is a minor concern but a simulation was run with side panels to observe how they would affect the deflection. The simulated deflection with the side panels was 0.04 in. This is negligible deflection for the design and meets the requirements.

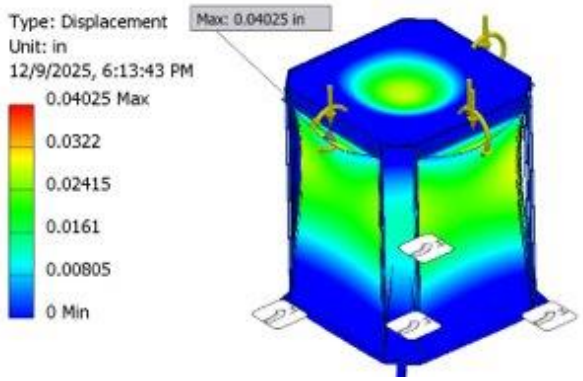


Figure 35: Station FEA with Panels

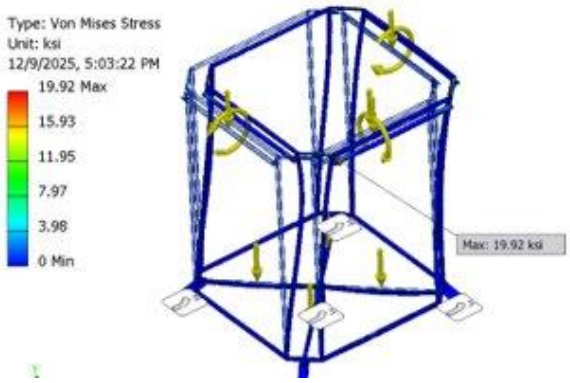


Figure 3336: Station FEA No Panels

The aluminum sheeting for the floor, roof, and solar panels will be 1/8" thick because these components need the stiffness and support to be held horizontally and support extra loads. The sheeting for the side panels will be 20 gauge due to these components not being load bearing but needing some minor stiffness.

The foot pads are 4.41 inches in diameter which is the diagonal of their 2x2 square base plus a 1in radius to give a large surface area to prevent sinking into the ground. The weight distribution is 17 pounds per square inch, which will not sink into the surface of mars. This is based on optimal terrain where the drifty surface is less than 6 inches thick and the surface below is rocky

or blocky as described by NASA in their geotechnical review. This surface can handle a pressure of 1000 kpa or 145psi.

The solar panels needed to meet the design requirements are 23in by 43in and collect 100 Watts of power each. They are extremely light with a total weight of about 5 lbs. However, they are flexible and will not support their own weight, so they are mounted on a 24in by 44in 1/8” thick aluminum sheet which weighs about 15 lbs. This sheet is attached to a bar that runs to the servos mounted on the solar brackets, allowing the panels to be adjusted to an optimal angle. The solar mounting bracket is made of 6061 aluminum and has a ½” thick support with ¼" mounting tabs and filleted welds which is the size needed to support the solar and maintain a factor of safety of greater than 1.4. According to FEA analysis the maximum stress is less than 8 ksi which is a factor of safety of greater than 3. The solar controller is built into solar panels and will follow the same process as the rover solar controls.

The batteries used in the station will be the same batteries used in the rover. The number of batteries would be governed by the number of rovers the station needs to service. For this design the station needs to service one rover so it will have the same battery capacity as the rover. There are two batteries in the rover, so there will be two batteries in the station. The batteries have internal battery management systems, so no external system is needed.

The ramp seen in Figure 37 needs to be able to level and align the rover so it can dock with the station. This will be made of 10 Gauge aluminum sheeting bent into a U channel with a slight V so the rover is perfectly aligned. The ramp is hinged to the station by the servos which allow it to be raised and lowered. These servos are mounted on the same brackets as the solar servos for ease of manufacturing.

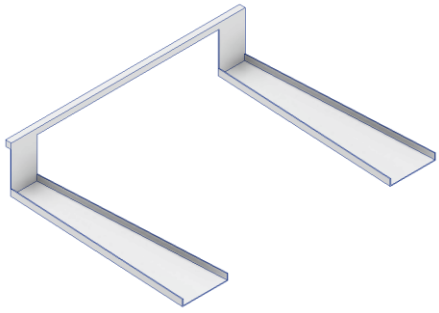


Figure 3734: Ramp Design

The charging connection seen in Figure 38 is supported by a ¼" plate and ¾" tubing because it is extremely important to mitigate the deflection so the charger will align correctly and not bind. The original design is not stiff enough according to the FEA analysis so a redesign and further analysis is needed as well as establishing the maximum allowable deflection, which will be based on manufacturing tolerances for the components and prototype testing. It was not possible to fully mathematically analyze this, which is why there are no definite answers. Prototype analysis is needed to establish tolerances and maximum allowable deflections which will drive the final design and additional support needed.

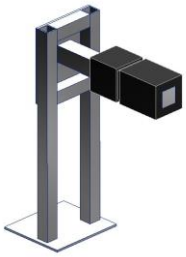


Figure 3835: Charging arm assembly

Charging Connection

The design of the charging interface required an evaluation of two primary connection methods: wireless energy transfer systems and direct contact wired connections. These two approaches represented the most viable options for delivering power from the charging station to the rover. Each method was assessed based on key project objectives, including regolith protection, charging speed, overall efficiency, and long-term reliability.

Wireless charging offered the advantage of simplified mechanical interfaces and reduced exposure to abrasive regolith. However, this method exhibited lower energy-transfer efficiency and significantly slower charging rates, making it less suitable for rapid power delivery. In contrast, a wired contact-based system, where conductive surfaces physically interface to allow current flow, provided much faster charging capabilities and substantially higher efficiency. These characteristics aligned directly with the primary goals of the project, which emphasized fast and efficient power transfer.

Although the wired approach introduces additional challenges in protecting the connection points from regolith infiltration, the benefits in performance outweigh the drawbacks. Future design efforts will focus on developing protective housing, sealing mechanisms, or self-cleaning interfaces to ensure that the wired connection remains reliable in dusty extraterrestrial environments.

Because minimizing the size of the charger is not a major concern, it can be made as large as is feasible. The maximum charging rate that could be feasible for the design is a 500Wh rover battery charged in under an hour. This would require 12 AWG wire or larger because 500 W at 24 V is 20.83 Amps and 12 Gauge is rated for up to 25 Amps. Selecting a contact that will fit wire this size and meet the requirements of being push to connect and flat. The contact that meets these requirements is found on McMaster-Carr and is ¼" wide.

Giving a ¼" buffer on each side for area to slide on, the charger becomes a ¾" by ¾" square tube made of TPU so it is flexible and can absorb contact with the rover without breaking. The ¾" height leaves room for the internal wires and angled contact. The spring constant for the assembly needs to be stiff enough to provide a secure seal that prevents regolith from entering the assembly, but relaxed enough that the rover can easily compress it and keep it in place without continuously applying power. The spring also needs 2 inches of travel to expose the contacts and allow the connection to be made. Based on these factors a spring constant of 20 lbs/in was selected with a free length of 4 inches to fit the design. The Compression Spring, 4" Long, 0.72" OD, 0.55" ID was selected from McMaster Carr which meets these exact

requirements. One spring is needed on each side of the connection. The charging arm assembly can be seen in Figure 39.

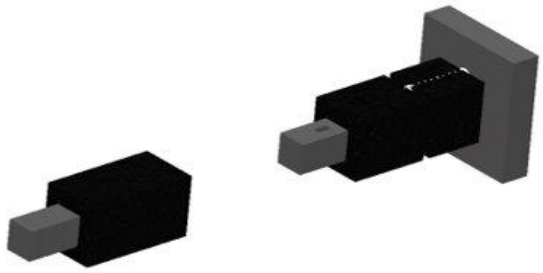


Figure 3936: Final Charging Arm Assembly

Final System Design

After completing the screening and scoring process, selecting the design to move forward with, and finalizing the detailed design, the final Rover and Station are shown below in Figure 40 and Figure 41.



Figure 4037: Final Rover Assembly

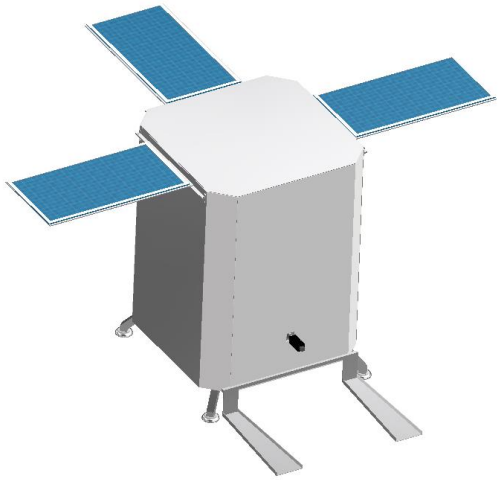


Figure 4138: Final Station Design

Redesigns

After the initial round of designing was completed, several changes were made to the solar protection assemblies. The first change made to these systems was the reduction of the motorized film roller consisting of an idler roller, motorized roller and a film return bucket. This system was overcomplicated and did not actually require the return bucket or the extra idler roller. To simplify this system for manufacturing, a single roller mounted on a bearing on one end and the round motor horn on the other side made this far more efficient and effective, while reducing space required and the number of components. This new system utilized a new and smaller servo motor that met the same requirements previously calculated, so no further analysis was required. To mount this new single motorized roller, a bracket was 3D printed for fast prototyping and ease of manufacturing. On the other side, a sealed ball bearing was pressed into the end of the roller pipe and mounted on an anchor pin. The anchor pin was then tack welded to a steal clip screwed to the frame. The new design is shown in figure 42.

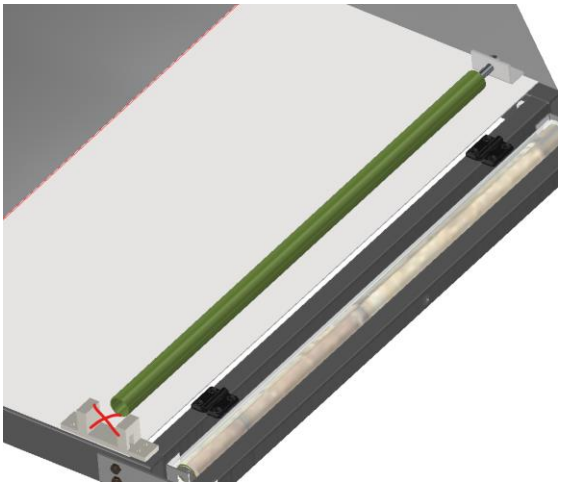


Figure 42: Updated Motorized Roller Assembly

The red ‘x’ marks the connection point of the servo motor to the 3D printed bracket to ensure the roller pipe is at an even level with the anchor pin on the opposite side. This motorized roller would roll up the damaged or dirty film that had previously covered the solar cell.

To ensure that the top solar cell did not deflect or become too susceptible to wind deflection and damage, as well as create a clean and tight fit between the protective film and the top cell, a square tube frame replaced the initial two aluminum tube supports that would support the cell as well as connect to the turning pipe shown in figure 43.

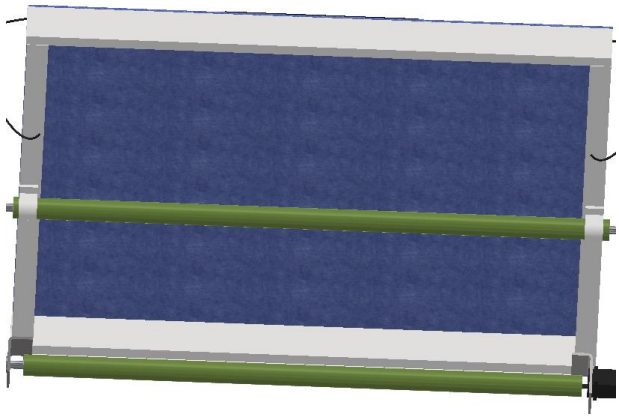


Figure 43: Top Solar Cell Frame

The addition added slight weight and material cost to the overall build but was acceptable due to its ability to support the film rollers and gear brackets that have yet to be discussed. The four 1x1.5” square aluminum tubes were to be welded together at the corners. This resulted in a far sturdier panel that could maintain its integrity in more harsh environments.

The next change that was made to the solar protection system was the connection between the motor that actuated the top solar cell, and the frame supporting the top cell. Prior to this, a servo motor was to be mounted on one end of the pipe supporting the top solar cell frame. This could no longer work because of the size constraints between the top sides of the frame, along with a mounting system that could not support this type of structural load. The new solution to this was a design change that involved mounting both ends of the top pipe on the same anchor pins used in figure 43 to mount the motorized roller. These anchor pins would also be tack-welded to steal clips screwed to the frame.

Figure 44 presents the new design to be implemented on both ends of the actuating pipe. The servo motor was then mounted on one end of the frame directly under the anchor pin with an aluminum linkage arm connecting the servo arm to the solar cell frame.

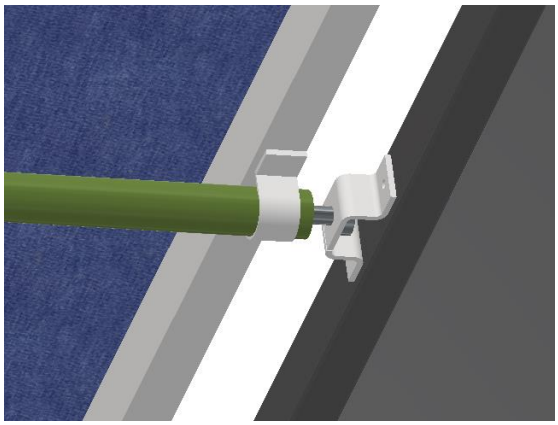


Figure 44: Actuating Solar Frame Roller

Figure 45 shows the mounting configuration that was used to hold the motor in place as well as connect the black motor arm to the solar frame with an aluminum linkage. This configuration allowed for a greater range of motion of the solar frame than was initially designed for. This design change was driven by a motor mounting system that came with the servo motor. This change was difficult to plan and design for in advance due to the minimal specs provided by the motor supplier (Amazon), but the linkage design was flexible and could accommodate this.



Figure 45: Solar Cell Motor Mount and Linkage

Another change that was made to the design was the addition of roller gears on all three rover solar cells to compress the protective film against the face of the solar cell. The purpose of this addition was to prevent the slight amount of force generated by lunar winds from pulling the film off the face of the cell, thus rendering the film useless. To accomplish this, a 3D bracket was designed and printed to support a pin that would allow for a small gear to roll with the film as it is pulled by the motor while still holding it to the face of the cell.

Figures 46 and 47 display the prints, pins, and gears to ensure the film is not pulled away from the face of the three solar cells on the rover. By installing two gears per solar cell carefully, the gear could roll with the film without puncturing holes in the film or preventing the motion of the roller motors.

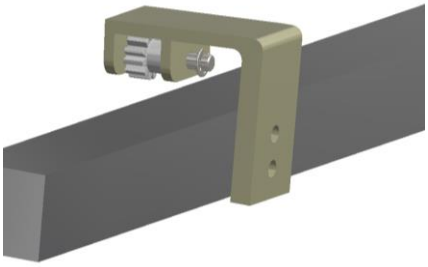


Figure 46: Film Gear for Top Solar Cell

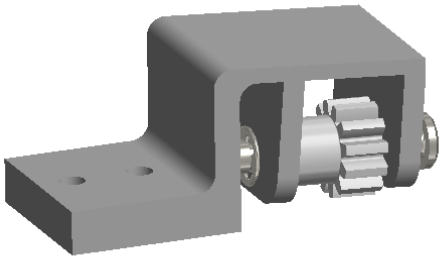


Figure 47: Film Gear for Front and Back Solar Cells

Design changes were made to the aluminum plate that connects the steering shaft to the suspension arms. This design change was to further protect the steering shaft and components from regolith during operation of the rover. This included a sealed ball bearing on top of the plate that was sized to the diameter of the steering shaft to provide horizontal support while permitting free rotation. The recessed groove on the previous design was replaced with a rubber lip seal that sat around the base of the steering shaft but allowed the thrust bearing to still sit flush against the plate. The plate was designed to have both the lip seal and sealed bearing press fit into the aluminum. Plate thickness was increased to ½" to allow for a bevel and deeper penetration of the weld bead. This was strictly for ease of manufacturing but naturally increased the strength of the plate as well. Threaded holes spaced in the plate's top face served as mounting holes for the steering servos and 3D printed spacer blocks to be mounted. Figure 48 shows the modified plate for the front rocker arms while figure 49 shows the assembly of the plate along with bearings, seals, and shaft.

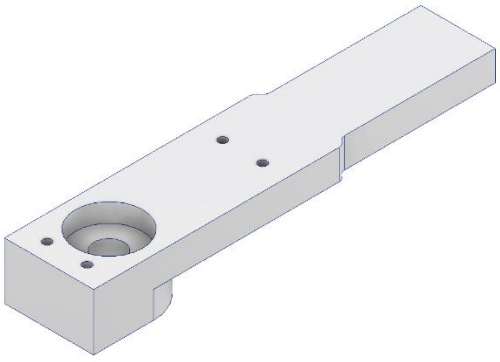


Figure 48: Modified Wheel Mounting Plate

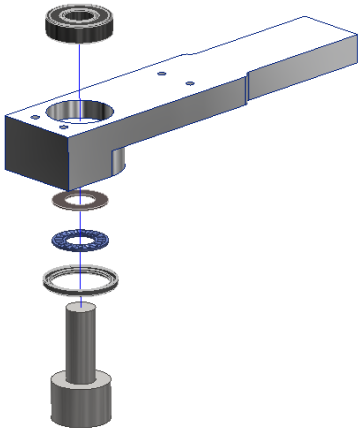


Figure 49: Mounting Plate Assembly

Aluminum spacer blocks for steering servo mounts were replaced with ABS 3D printed blocks with through holes to connect the servo to the mounting plate via 10-24 bolts. These screws were the optimal diameter to fit the servo mounting holes and the spacer block was designed for bolt clearance. A groove has also been cut on the top of the block to allow the servo motor to sit flush on the face. To allow for rotation and clearance of the horn and servo connector, an arch was placed in the face of the block. This block is for spacing the servo motor off of the mounting plate and does not see any untypical forces, so 3D printed ABS plastic was a simple and cost-effective choice. Figure 50 shows these spacer blocks which were used twice on all four steering servos.

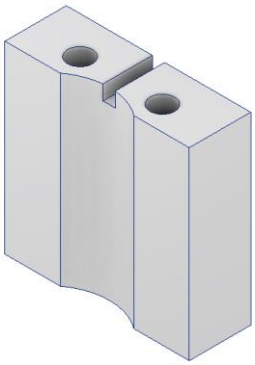


Figure 50: Servo Spacer Blocks

A new design was made for connecting the steering shaft to the servo motor. These motors came with 1 inch round anodized aluminum servo horns that would be used for the connection. M2.5 bolts threaded into 8 holes around the horn which would be used to connect to the shaft. For the interface between them, a stainless-steel disk with 8 through holes corresponding to the bolt positions was made to be welded onto the crown of the steering shaft. Figure 51 shows this connection disk along with a bottom neck for alignment on the shaft.

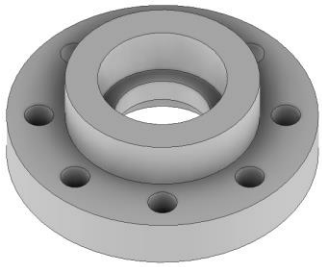


Figure 51: Servo Connection Disk

For wire protection and additional regolith protection of steering components, a 3D printed ABS cover was designed to slip over top of the wheel mounting plate and steering servo. This design was self retaining through tight tolerances and friction to create a tight seal. These steering covers can be seen in figure 52.

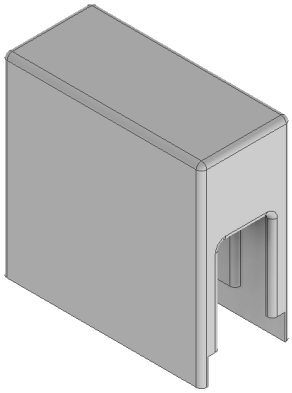


Figure 52: Steering Cover

To replace the aired rubber tire that comes standard on the selected hub motor, a 3D printed wheel design was created using a combination of PLA and TPU to demonstrate a usable wheel on the surface of the moon and mars where an aired tire would not be applicable. This design in figure 53 would not be put on the rover for testing to avoid damage of the electric hub motors but instead provided a concept of tire tread that would optimize traction.



Figure 53: Rover Wheel Demonstrative Concept

The design changes done to the station were: reducing the overall size, resizing the tubing and sheet metal, changing the angle of the legs, changing where the charger supports were connected, adding a hinged door for access, and changing the solar frame from sheet metal to tubing.

The overall size was reduced from 4'x4'x5' to 32.5"x32.5"x38". The size was changed because the station does not need a full size RTG for the testing required, it also increased the ease of transport after manufacturing by making the station lighter and easier to carry. Additionally, the extra size was not needed to fit the solar panels required for the needed power input.

The tubing used to build the station was changed from ¾" square 1/16" thick to 1" square 3/32" thick. This was due to the original size not being stocked locally, and the thicker tubing being much easier to weld. This reduced the cost of purchasing stock and the likelihood of failure during manufacturing. The corners were also changed to be the same tube size as the rest of the station. This also was because it was much easier to procure but had the disadvantage of needing angles to be cut in the ends of all 16 of the hoop tubes instead of just the 8 corner pieces. The sheet metal was changed to a consistent 1/16" because with the supports and the increased size of the tubing there was no longer a need for the additional stiffness and strength from the aluminum sheeting. This allowed costs to be reduced by decreasing and standardizing the size.

The legs of the station were changed from a five leg design with the outer legs angled outward to a 4 leg design with all legs straight. This was because without the weight of an RTG the center leg was not needed.[4] Additionally, this increased ease of manufacturing and decreased points of failure.

The charger supports were changed from a vertical cantilever design to a horizontal design supported on both ends. This increased the strength of the charger and decreased the amount of material needed, making it both cheaper and stronger.

A hinged access door was added to the side of the station making assembly of electronic components easier and allowing maintenance on the internals to be performed without having to remove the full panel. This was done by cutting the panel just below the solar bracket and adding a hinge at the bottom so the door can swing down like a ramp. The hinge was placed at the bottom due to a lack of suitable mounting points on the sides of the panels.

The frame for the solar was changed from a sheet of steel to aluminum tubing. This reduced weight, which reduced the forces experienced by the servo motor and the station. Additionally, the tubing is stiffer than the sheet metal preventing the solar panel from sagging. The frame is made from ½" square tubing 1/16" thick. This frame connects to a 1" square tube that runs from the servo to the hinge. The tubing in this section is larger because of the high amount of torsion from the servo.

A few small design changes were made to the charging connection. The biggest change was to eliminate the springs and linkages in the rover side of the charger. Instead a simple V contact was used that would sit below the hole, but be able to push out of the way when the plunger is depressed. The station side then became a flat pad that the V contact would rest on allowing power transfer. The exploded assembly of the updated parts is shown in figure 54.

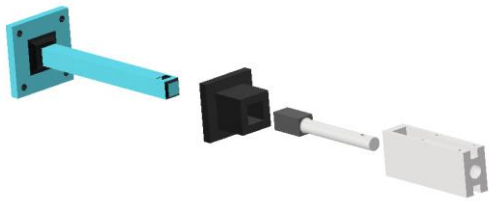


Figure 54: Modeled Charging Connection

Manufacturing

Rover Body

To ensure that the frame of the rover was solid and completed on time, the aluminum tubing was purchased and then delivered to a welding company to be completed early in the semester. Once the frame was welded and acquired, further manufacturing commenced.

Aluminum sheeting was purchased in large 4x10’ sections that were cut down to specified sizes by utilizing the press break located in the engineering buildings on campus. This allowed for the simple square and triangular shapes in figure 55 to be cut by the team, both cost effectively and accurately to meet dimensions and tolerances.



Figure 55: Frame, Sheet Metal, and Subsystems

Steal and aluminum clips used on the rover to support the front bumper tube and all rollers with their respective anchor pins were produced by the team in the labs on campus by cutting sheet metal with the press break and bent to 90-degree angles. The drill press located in the auxiliary lab was used to add holes to all clips to create sufficient tolerances and align the pipe axis of each roller shown in figure 56.



Figure 39: Top Film Idler

Once the Schedule 40 pipe in figures 56 and 57 was procured for the film rollers and for the top actuating frame, the pipe was cut into specified sections on a vertical band saw in one of the labs. Once cut to size, both ends of each piece were reamed until the ball bearings were able to be pressed into the anchor sides, and a pipe cap was able to fit into the other. With the pipe caps installed, the circular horns of the servo motors were screwed into the cap so that the motor could be aligned with the axis of the pipe.



Figure 57: Actuating Frame Mount

Figure 58 shows both the top pivoting panel welds done by the team as well as the latches installed on the front and back sheets to allow for easy access to the storage compartments housing the electrical components. All sheet metal pieces were installed on the rover by using self-tapping screws to minimize the number of required welds.



Figure 58: Top Pivoting Frame

The top pivoting frame was fixed to the supported roller by fastening routing clamps around the pipe by bolting them to each side of the frame as is seen in figure 59. At the bottom of this figure, the front bumper can be seen better in figure 60 bolted to a supporting clip and screwed to the frame.



Figure 59: Rover Body



Figure 60: Bumper and Film Idler Tolerance

This configuration allowed for the bumper to be offset from the front of rover frame just far enough to allow for the preloaded film roller to fit and not interfere with either. Additionally, figure 61 below shows more clearly the ribbed shoulder support that was welded onto the frame by the same company that welded the rest of the rover frame.



Figure 61: Ribbed Shoulder Joint

This joint in figure 20 was aluminum angle produced by McMaster-Carr and cut to the specified length by the team. Once cut to length using a horizontal band saw, holes were drilled into one of the faces to match the slotted hole pattern of the shoulder ball bearings. These shoulder bearings would support the pivoting movement of the suspension arm, thus holding the weight of the rover as it navigates uneven terrain. Ribs were added and welded on as well to provide additional strength and stiffness since any deflection in this shoulder joint would mean adding great stresses to weaker parts of the suspension.

Additionally, figure 62 shows the linkage arm allowing for the motor arm to rotate the frame despite being offset from the axis of the pipe. The dimensions and connection point of this linkage arm were determined by trial and error to maximize the range of motion.



Figure 62: Top Frame Connections

Figures 63 and 64 show the 3D printed brackets, pins, and gears used to press the film against the face of the solar cells.



Figure 63: Front and Back Panel Roller Gear



Figure 64: Top Panel Roller Gear

Suspension and Drive Train

The rocker-bogie suspension system was manufactured out of 6061 aluminum and was separated into multiple segments for manufacturing. The rocker arms were comprised of the central block seen in figure 65 which was laser cut out of 1.25” thick 6” long and 5” wide aluminum plate while the front and rear legs of the rocker arm were milled down to size from 1.25” x 1.25” square tubing that was originally 36” long. The central blocks were also tapped with ¼-28 threads on top for linkage attachment and 5/8-11 threads on the face to attachment to the central bearing. The bogie arms were made of the same square tubing along with the bogie block. For assembly, aluminum MIG welding was used with a specialized spool gun to fuse the assemblies together. Deep bevels were cut into the ends of the components to maximize weld penetration and create a uniform and solid aluminum suspension assembly.



Figure 65: Rocker Blocks

The redesigned aluminum wheel mounting plates were CNC milled to obtain the circular geometries and tight tolerances required for alignment as seen in figure 66. Once milled, these plates were subsequently beveled and welded to the ends of the rocker and bogie arms to complete

the suspension structure. Finally, the radial bearings and lip seals were press fit into the wheel mounting plates. The fully completed rocker arms are seen in figure 67.



Figure 66: Wheel Mounting Plates



Figure 67: Completed Rocker Arms

The four wheel brackets were manufactured from blocks and rods of 304 stainless steel. Three rectangular rods were machined to size and slotted for the hub motor shafts with a mill, arranged into a U shape, then welded together to form the main bracket. The steering shaft was machined on a lathe to size then welded to the center of the bracket. The completed wheel brackets are shown in figure 68.



Figure 68: Welded Stainless Wheel Brackets

Wheel brackets were then able to be inserted into the rocker and bogie arms through the bearing and lip seal embedded in the wheel mounting plate with the thrust bearing and bearing race. To retain the bracket and to ensure no vertical stress was experienced by the servo motor, a snap ring

was inserted into a groove of the steering shaft to prevent it from sliding back through the radial bearing. This assembly is seen in figure 69 with the bracket attached to the rocker arm.



Figure 69: Rocker and Wheel Bracket

The stainless-steel disk used to interlock the servo horn and steering shaft was created on a lathe to form the shape required. Then using a mill, the 8 through holes were drilled to align with the servo horn. These disks were aligned on top of the steering shaft and subsequently TIG welded to fully bond them with the shaft.

The rocker and bogie arms were then fitted with the servo spacers and servo motors attached by 10-24 bolts to the wheel mounting plate. M2.5 bolts attached the servo horn to the stainless-steel disk to create a steerable wheel bracket. The electric hub motors were then attached to the wheel brackets by the threaded shaft to lock the motors in place. Figure 70 and figure 71 show the steering mechanism of the suspension entirely assembled.



Figure 70: Steering Controls and Motors

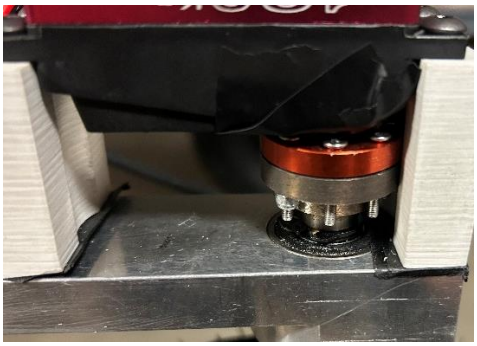


Figure 71: Servo Connection to Steering Disk

The rocker arms and bogie arms were then attached to each other using a 3/8” shoulder bolt at the back of the rocker arm and center of the bogie arm spaced by a PTFE washer to allow a tight and rigid connection while allowing rotation of the suspension. The rocker arms were then attached to the main bearings of the rover by a ¾” shoulder bolt that is threaded into the block of the rocker. This provided a pivot point for the suspension to rotate. To maintain the rover’s upright position and allow for suspension travel, the center differential bar was cut to length on the mill to 35.5” with a ½” hole drilled into the center for the pivot point. The ends of the differential bar were drilled and tapped for ¼-28 threads to attach the linkage bars of the suspension. This differential bar was then attached to the center of the rover frame using a ½” shoulder bolt and again a PTFE washer to reduce friction and provide a rotational degree of freedom. 6” linkage bars with ball joint linkages were subsequently attached to the top threads of the rocker block and the end threads of the differential bar. This completed the suspension as seen in figure 72 which maintained the rover’s stability and allowed for individual wheel and suspension travel for optimal ground contact and balance. 3D printed ABS covers were added over the steering controls to add additional protection to the wiring and prevent dust from entering the mechanisms.



Figure 72: Final Suspension and Drive Train

To avoid damaging the hub motors and risk compromising the drivability of the rover, the aired rubber tires were left on for rover functionality. A demonstrative wheel was manufactured out of 3D printed PLA and TPU and attached to an extra purchased hub motor. This was to display a potential wheel design that could be used on this project. Figure 73 shows this wheel tread design on the display stand.



Figure 73: Demonstrative Wheel Design

Electrical

To connect the solar panels to the battery system, a solar charge controller shown in figure 74 was required to regulate voltage and ensure safe charging operation. The three solar panels were connected in series, with each panel having a maximum output voltage of approximately 29 V. The selected solar charge controller was rated for operation up to 100 V. With all three panels connected in series, the maximum possible system voltage was approximately 87 V, providing sufficient headroom to maintain safe and reliable operation within the charging system.



Figure 74: Solar Controller and Internal Wiring

The rover steering system utilized 160 kg servo motors mounted at each corner of the rover. This configuration enabled four-wheel steering capability, including quad steering and zero-point turning. To allow each servo to operate independently, dedicated a 5V positive and negative power wires were connected to the load side seen in figure 75 of the solar charge controller, while individual signal wires were connected to the BEC output channels on the flight controller.

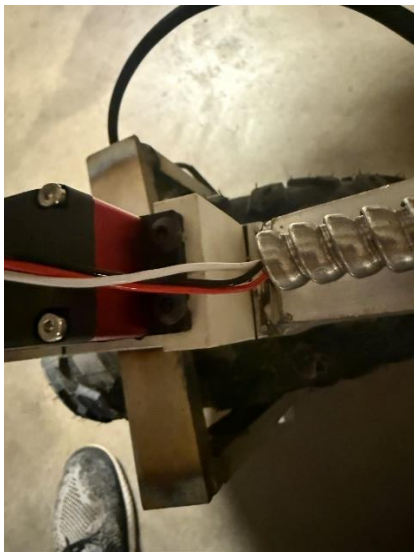


Figure 75: Steering Servo and Conduit

The rover propulsion system used 350 W internally geared hub motors. These motors required a smart electronic speed controller, commonly referred to as a VESC, for proper operation and control. Each motor was connected to the VESC through three phase wires responsible for motor power delivery, along with five Hall sensor wires used for rotor position feedback and smooth motor operation figure 76. All connections were carefully installed with the correct orientation to ensure proper motor rotation and performance. After wiring was completed, the Hall sensors were calibrated and configured, and the three-phase motor connections were verified to ensure reliable operation.

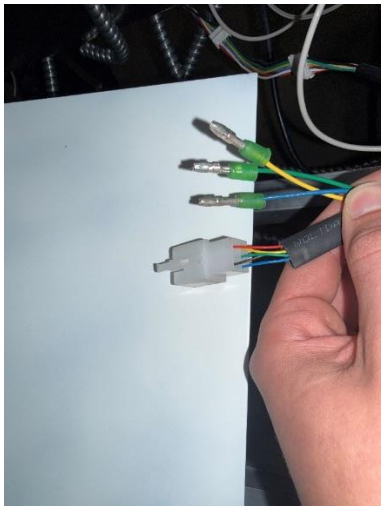


Figure 76: VESC Connections

The flight controller was connected to the VESC to control the amount of power delivered to the hub motors at any given time. To establish communication between the two systems, a ground wire, a 5 V positive wire, and a signal wire were connected from the flight controller's BEC output to the VESC input as shown in figure 77. This allowed the flight controller to transmit throttle and control signals that the VESC could interpret and use for motor control.

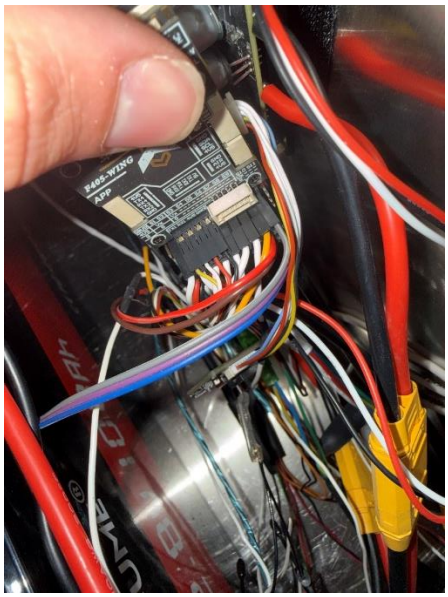


Figure 77: Flight Controller and Internal Wiring

Station

The station was manufactured using 1”x1” tubing 3/32” thick. The cut list was 8 lengths of 36", 8 lengths of 24” with 22.5 degree angle cuts, and 8 lengths of 6” with 22.5 degree angle cuts. The 6” and 24” pieces were assembled into octagons and welded together using a TIG welder as shown in figure 78.

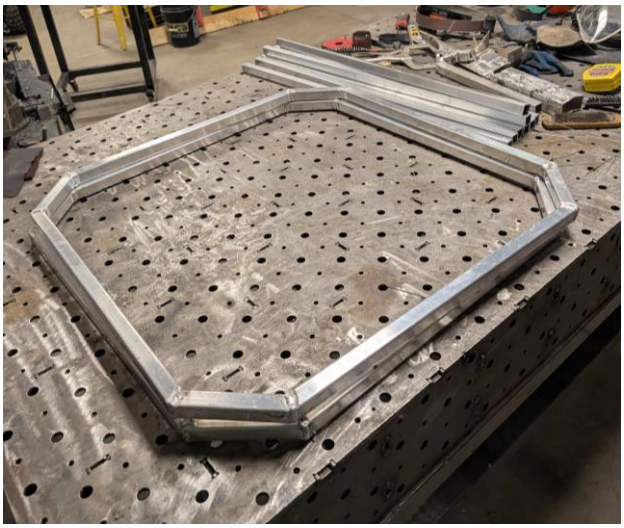


Figure 78: Top and Bottom Frame of Station

These two octagons were then connected using the 36” lengths at the corners and welded using the same process. The completed main station frame is shown below in figure 79.



Figure 79: Welded Frame of Station

The station must hold the weight of the batteries, RTG, and other electrical components. To support these loads cross members were added from corner to corner on the bottom as designed. Additionally, supports for the charging connection were added to prevent the charger from failing. The legs were made using a 1” hollow tube welded to a 1” square cube to support the nut for the foot pads. The side, roof, and floor panels were then cut from 1/16” aluminum sheeting and screwed to the frame using self tapping screws shown in figure 80.



Figure 80: Welding of Station

To support the solar panel assemblies angle iron brackets were created to support the servo motors using ¼" thick aluminum 1 ½" wide, and welded to the vertical bars of the station. The opposite side of the assembly is supported by a hinge screwed to the other vertical support. Support frames for the solar panels were made from 1/16” square aluminum tubing ½"x ½". The frames were

welded together and holes were drilled in the ends to connect to the servo arm. The empty frame attached to the servo and station is seen in figure 81.



Figure 81: Station Solar Frame

The solar panels were attached to the frames using adhesive. Then the charging connection was added to the front of the station and the rest of the side panels were assembled. The final station assembly is shown below in figure 82.



Figure 82: Finalized Station

The internal electrical components of the station consisted of a flight controller, two batteries, and a solar controller. The solar controller manages the power input from the solar cells and controls the output of the battery to the flight controller, charging connection, and servo motors. The flight controller has 3 signal wires one connected to each of the servos. The flight controller assembly is shown in figure 83.

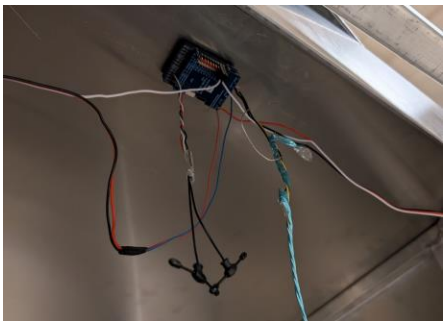


Figure 83: Flight Controller on Station

Figure 84 shows the station with the access door open revealing the internal components of the station.



Figure 84: Station Door and Interior

Charging Connection

The charging connection parts were manufactured with 3D printed PLA. The springs were procured and added to the assembly. A mounting bracket was created for the rover side using sheet aluminum and square tubing to be attached to the bumper of the rover. The final assembly of both the station and rover sides of the connection is shown in figure 85.

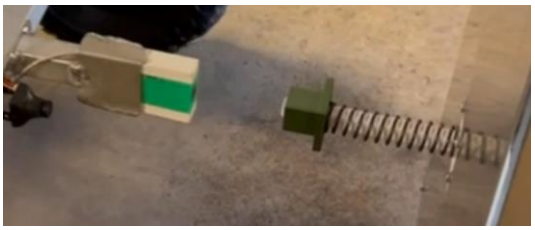


Figure 85: Rover to Station Charging

4. Laboratory Test Results

The initial testing phase for the rover and station focused on verifying that the receiver could successfully communicate with the transmitter. This was accomplished using the software INAV.

Through INAV, the receiver and transmitter were properly connected, and the system was able to display the input signals received over radio waves from the transmitter. This confirmed that the communication link between the two components was functioning as intended.

Once the first round of solar cells and LiFePo4 batteries arrived, testing was done to determine the actual power output of the solar cells through the solar controller. This was completed by setting two solar cells out on the pavement on a sunny day while connected in series. By running the two solar cells through the solar controller and then into the batteries, the power and charging rate of the batteries from the cells were determined. The maximum amps were read to be roughly 6.5 A, and a maximum voltage of 65 V, however, both values fluctuated. These values were slightly less than the sum of the rated values of each panel added together, although this was to be expected due to the season and location the testing took place.

Another system that was tested was the top pivoting frame. Once the frame was mounted on the rotating pipe and the linkage arm was connected to the motor arm and the frame, the servo cables were extended to the battery. This was done to test the speed of rotation, sensitivity of the controller, and the range of motion. By manually leveling the pivoting frame and then pressing the designated controller button one direction at a time, the bounds could be set to prevent over rotation. After several rounds of adjusting the range bounds and speed of rotation, the top panel tilted at a slow and consistent speed over a range that allowed for 50-degrees of rotation in either direction. This maximum range of rotation was about 20-degrees more than what was designed for initially, proving a very successful design and test.

To test the hub motors, a test stand was built to support one wheel and allow it to spin freely. By connecting the motor to a power source and controlling it through the VESCs and flight controller, the motor could be tested. The left joystick was set to control the forward backward movement of the wheel in the stand. Even though this process only tested one motor, the same settings, speed rate, input channel to the controls, and other settings could be copied to the other hub motor channels on the flight controller.

Steering systems were tested once the wheel brackets had been attached to the suspension arms. Initially, a free rotation test by hand was done to ensure the bracket and shaft rotated smoothly without any slop or play in the horizontal direction. This also ensured that there was no binding or rough spots that could cause failure later on. All four brackets turned smoothly so next step was to test the steering with the entire steering mechanism installed. Once again, the wheels and brackets were able to turn smoothly with the servo providing the force needed to precisely turn the wheels, proving a successful steering system.

The rocker bogie suspension design was tested in multiple stages. Once installed and before the weight of the rover body was placed on the suspension, movement tests were conducted by hand by pushing and pulling up on the arms to demonstrate the differential bar travel abilities. The system responded as designed and as on arm traveled upwards, the differential bar would offset the force and push the other side down to keep the rover stable. Then the rover was grounded and all of the weight was supported by the suspension. The arms were lifted and placed on cinder blocks to test different climbing angles and lifting distances. Again, the suspension performed superbly and maintained ground contact in all positions tested. Figure 86 demonstrates this test as it was conducted.



Figure 86: Rover Suspension Test

To test the charging connection a multimeter was used to measure the continuity of all contacts to their respective wires. Then the connection was mated and continuity was tested again between all wires to ensure the charging connection was able to transmit power through the correct wires and to ensure there was an open circuit between all the other wires so no shorting would occur. All of the contact testing resulted in the correct continuity pattern. After the connection was assembled onto the station and rover it was tested to ensure the rover could align and connect the charger. The rover was able to push the connection together and complete the charging circuit as seen below in figure 87. The connection worked; however, it was difficult to align. The suspension on the rover would rock causing the height of the charger to change and creating misalignment. The connection was beveled slightly to allow some room for error, but it still needed to be within an eighth of an inch or it would not mate.



Figure 87: Rover Docking to Station

Testing the station solar panel actuation was done by first testing the servo motor operation separate from the assembly then once operation was confirmed, the system was assembled and tested for functionality. The solar panels actuated as they were intended to but had a reduced range of motion due to the hinge binding once the solar panel approached 90 degrees in figure 88.



Figure 88: Actuating Solar Testing

5. Conclusions

After project completion and testing it was determined that the rover and station performed their necessary duties to meet the project objectives. The rover and station were able to demonstrate charging which allows for rovers on the moon and mars to be charged. The features were mostly dust proof with the largest issue coming from the sheet metal not fully sealing. The rover demonstrated the ability to climb over steep and uneven surfaces while maintaining traction and stability, limited only by the torque of the motors. The size constraints were met with the rover form factor being 53”x72”x60” WxLxH. The weight of the rover was much less than the 500 lb limit with the rover weighing 150 lbs, with an actual MMRTG this weight would increase about 50 lbs but still easily meet the requirements. The rover and station both have 2560 Wh of battery capacity which exceeds the required 2000 Wh needed. The rover’s top speed is 5 mph allowing it to quickly reach rovers in a critical power state to revive them, or to ferry power from the station to working rovers.

The rover and station meet the basic design objectives, but a few issues arose during testing and operation. While driving the wheels had a tendency to camber which added additional stress to the drivetrain and suspension components, four of the eight servo motors failed during testing, two of the six hub motors failed to operate, the charging connection was difficult to align, and the solar film did not fully protect from dust due to parts being in the way. Despite these minor issues the rover and station operate as intended. The project was successful and all tasks were able to be completed.

6. Future Work and Recommendations

Cambering

During testing and operation, it was observed that the suspension system would twist causing the front wheels to bend inwards then due to the force of driving forward the whole suspension system would tilt wheels inward causing a positive camber. The opposite would happen when the rover was driven in reverse. It was determined this was due to the wheels not being aligned in a single plane which creates a bending moment around the main pivot. The main pivot could handle the loading but the single shaft would bend creating this deflection. To fix this the drive wheels should

all be aligned in the same plane to prevent the bending forces and the main pivot shaft should be larger and dually supported to decrease the amount of flex that occurs.

Servos and Hub Motors

During testing and operation, some of the servos and hub motors failed. This was possibly due to the torque required for some tasks creating high currents, or the batteries producing too much voltage. To fix this, better motors should be used, and the torque required to complete tasks should be measured to ensure the motors can handle it. Economical motors were selected for this project but due to how critical they are to the operation of the rover and station higher quality motors should have been used to prevent failure.

Charger alignment

The charging connection worked but was not easy to connect. To improve this connection, a design change is needed to make alignment and mating easier. The simplest solution would be to make the end of the rover connection a larger funnel shape allowing for more room for error. The connection can also be made from a more flexible material which will allow the connection to properly mate even when they are not perfectly aligned. The downside to the funnel shape is it may collect regolith causing wear or failure of the contacts to touch. This would require testing with regolith simulant to determine the optimal shape of the connection.

Solar Film

The ETFE solar film selected for this project worked very well and allowed for charging capabilities that nearly reflected the charging rate of the solar cells prior to anything covering them. However, despite the two roller gears added to each solar panel, a small gap between the film and the face of the panel did become apparent. This was due to two factors. First, the rover was driven outside on a windy day, causing greater forces to act on the edge of the film and pull it away from the panel than what it would experience on any lunar surface due to the far denser atmosphere of Earth. Second, the panels had a compartment protruding from the top of the face with positive and negative leads coming out to connect to the batteries. While necessary, these leads pushed out away from the face and against the film, causing a gap at the top of each panel. This problem was most evident on the top actuating solar panel as it rotated and the leads were pulled.

Both problems could be mitigated by adding some sort of routing clamp or bracket that held the leads in place straight out to the sides of the face of the panel and mounted just outside of the film. Additionally, rather than having one roller gear on each side of each solar cell, two or even three roller gears could be added to entirely remove any chance of dust or regolith from getting between the film and the solar cell. Lastly, a weak radial spring could be added to the idler roller side that held the new clean film but wouldn’t be so strong as to over torque the motor. This would ensure that slack is not created by storm effects, vibration induced by travel, or over-rotation of the idler caused by the motor on the other end rolling up the film.

7. References

[1] “Mars Science Laboratory Curiosity Rover – Mars Missions – NASA Jet Propulsion Laboratory,” NASA JPL. Accessed Dec. 12, 2025. [Online]. Available: https://www.jpl.nasa.gov/missions/mars-science-laboratory-curiosity-rover-msl/

[2] NASA, “NASA-STD-5009C: Nondestructive Evaluation Requirements for Fracture-Critical Metallic Components,” Office of the NASA Chief Engineer, Aug. 3, 2023. [Online]. Available: https://standards.nasa.gov/sites/default/files/standards/NASA/C/0/2023-08-03-NASA-STD-5009C-Approved.pdf.

[3] NASA, “NASA-STD-5001B w/CHANGE 2: Structural Design and Test Factors of Safety for Spaceflight Hardware,” National Aeronautics and Space Administration, Approved Aug. 6, 2014; Administrative/Editorial Change Oct. 5, 2016. [Online]. Available: https://standards.nasa.gov/sites/default/files/standards/NASA/B-w/CHANGE-2/2/nasa-std-5001b_w_change_2.pdf

[4] R. Bechtel, “Multi-Mission Radioisotope Thermoelectric Generator (MMRTG).” Accessed Dec. 12, 2025. [Online]. Available: https://www.nasa.gov/wp-content/uploads/2015/08/4_mars_2020_mmrtg.pdf?emrc=35c41b